(12) INTERNATIONAL APPLICATION PUBLISHED UNDER THE PATENT COOPERATION TREATY (PCT)

(19) World Intellectual Property Organization
International Bureau

(43) International Publication Date
11 October 2018 (11.10.2018)

WIPO | PCT

(10) International Publication Number
WO 2018/184056 A1

(51) International Patent Classification:
G01R 33/20 (2006.01) *A61B 5/055* (2006.01)

(21) International Application Number:
PCT/AU2017/050294

(22) International Filing Date:
05 April 2017 (05.04.2017)

(25) Filing Language: English

(26) Publication Language: English

(71) Applicant: **THE UNIVERSITY OF QUEENSLAND** [AU/AU]; The University of Queensland, St Lucia, Queensland 4072 (AU).

(72) Inventors: **STÄB, Daniel**; 3/15 Whitmore Street, Taringa, Queensland 4068 (AU). **BARTH, Markus**; 196 Indooroopilly Rd, St Lucia, Queensland 4067 (AU).

(74) Agent: **DAVIES COLLISON CAVE PTY LTD**; Level 10, 301 Coronation Drive, Milton, Queensland 4064 (AU).

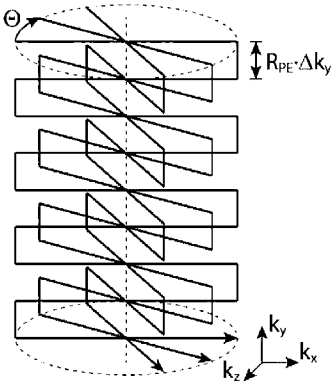
(81) Designated States *(unless otherwise indicated, for every kind of national protection available)*: AE, AG, AL, AM, AO, AT, AU, AZ, BA, BB, BG, BH, BN, BR, BW, BY, BZ, CA, CH, CL, CN, CO, CR, CU, CZ, DE, DJ, DK, DM, DO, DZ, EC, EE, EG, ES, FI, GB, GD, GE, GH, GM, GT, HN, HR, HU, ID, IL, IN, IR, IS, JP, KE, KG, KH, KN, KP, KR, KW, KZ, LA, LC, LK, LR, LS, LU, LY, MA, MD, ME, MG, MK, MN, MW, MX, MY, MZ, NA, NG, NI, NO, NZ, OM, PA, PE, PG, PH, PL, PT, QA, RO, RS, RU, RW, SA, SC, SD, SE, SG, SK, SL, SM, ST, SV, SY, TH, TJ, TM, TN, TR, TT, TZ, UA, UG, US, UZ, VC, VN, ZA, ZM, ZW.

(84) Designated States *(unless otherwise indicated, for every kind of regional protection available)*: ARIPO (BW, GH, GM, KE, LR, LS, MW, MZ, NA, RW, SD, SL, ST, SZ, TZ, UG, ZM, ZW), Eurasian (AM, AZ, BY, KG, KZ, RU, TJ, TM), European (AL, AT, BE, BG, CH, CY, CZ, DE, DK, EE, ES, FI, FR, GB, GR, HR, HU, IE, IS, IT, LT, LU, LV, MC, MK, MT, NL, NO, PL, PT, RO, RS, SE, SI, SK, SM, TR), OAPI (BF, BJ, CF, CG, CI, CM, GA, GN, GQ, GW, KM, ML, MR, NE, SN, TD, TG).

Published:
— *with international search report (Art. 21(3))*

(54) Title: MAGNETIC RESONANCE IMAGING METHOD AND APPARATUS

Fig. 4B



(57) Abstract: A magnetic resonance imaging method for imaging an anatomical region of a subject, the method comprising: generating an imaging field, the anatomical region being provided in an acquisition space within the imaging field; generating multiple acquisition sequences, each acquisition sequence including an RF excitation pulse, and gradient field pulses configured to generate a readout trajectory in *k*-space, each readout trajectory including a number of scan lines extending in a frequency encoding direction and spaced in a second phase encoding direction along a phase encoding axis, and the multiple acquisition sequences generating a plurality of readout trajectories extending over at least part of an acquisition space, the readout trajectories being rotated at least partially about the phase encoding axis; acquiring echo signals from the readout trajectories for each of the multiple acquisition sequences to generate k-space data; and, processing the *k*-space data to generate at least one image representation of the anatomical region.

WO 2018/184056 A1

MAGNETIC RESONANCE IMAGING METHOD AND APPARATUS

Background of the Invention

[0001] The present invention relates to a magnetic resonance imaging (MRI) method and apparatus, and in one particular example, to a magnetic resonance imaging method and apparatus suitable for use in susceptibility mapping.

Description of the Prior Art

[0002] The reference in this specification to any prior publication (or information derived from it), or to any matter which is known, is not, and should not be taken as an acknowledgment or admission or any form of suggestion that the prior publication (or information derived from it) or known matter forms part of the common general knowledge in the field of endeavour to which this specification relates.

[0003] With the advent of ultra-high field MRI scanners in clinical research, Quantitative Susceptibility Mapping (QSM) has recently gained increasing interest because of its potential to assess subtle tissue changes underlying neurological pathologies/disorders. It offers potentially novel insights into tissue composition and disease related tissue changes in the human brain. As a result it can be considered as a novel biomarker based on the magnetic properties of tissue, for example, as it helps visualize microbleeds and differentiate them from calcifications. It can also potentially be used for measurement of iron and myelin concentrations in the human brain, as well as electrode placement planning for deep brain stimulation. QSM and magnetic susceptibility based MRI in general profit disproportionately from scanning at ultra-high field due to the increase in signal-to-noise ratio (SNR) and white matter–grey matter contrast. Compared with lower field strengths (<3 T), improvements for glioma treatment response MRI and MRI of microbleeds, as well as the characterization of multiple sclerosis (MS) lesions, have been demonstrated.

[0004] The current standard acquisition technique for structural T_2* weighted, susceptibility weighted MRI and QSM is a three-dimensional (3D) spoiled gradient-echo (GRE) sequence with Cartesian sampling. It can be used with high spatial resolution to detect small structures

and lesions and has performed well with respect to SNR and stability. However, the long measurement time can be problematic in terms of head motion during the scan. This is particularly the case in clinical populations, such as Alzheimer's and Parkinson's disease, where involuntary head motion is more common than in healthy control participants. The image acquisition can be accelerated using partial Fourier imaging, elliptical scanning and parallel imaging. However, these methods come with a reduction in SNR due to the acquisition of a reduced amount of *k*-space data.

[0005] In addition, parallel imaging – such as simultaneous acquisition of spatial harmonics (SMASH), sensitivity encoding (SENSE) or generalized auto-calibrating partially parallel acquisitions (GRAPPA) – introduce some noise amplification during the reconstruction process, characterized by the so-called geometry factor. To a certain extent, this effect can be mitigated by shifting the sampling positions in *k*-space so that the coil sensitivity variations can be exploited more efficiently in multiple dimensions, resulting in a more robust parallel imaging reconstruction.

[0006] Another strategy to shorten the acquisition is to use echo-planar imaging (EPI), which increases the efficiency by a factor of 10–100. It is mainly limited by the desired echo time (T_E) – and as such the gradient performance. Moreover, the T_2* of the tissue of interest can be restricting, since long readout trains can lead to spatial blurring. Further limitations include geometric distortions and signal dropouts, which are typically worse at higher fields and become more severe at ultra-high field strength.

[0007] US2012/0220858 describes an MRI-based system includes an MRI scanner having a first axis and a first plane perpendicular to the first axis, a pulse sequence module configured to provide a 3D pulse sequence to the MRI scanner, and a control module configured to instruct the MRI scanner to conduct radial *k*-space samples having N second planes that each are perpendicular to the first plane and through which the first axis passes, N being an integer greater than 1. The 3D pulse sequence instructs the MRI scanner to a radio-frequency (RF) pulse, conduct a gradient readout in the first plane, and conduct a gradient readout in one of the N second planes.

Summary of the Present Invention

[0008] In one broad form an aspect of the present invention seeks to provide a magnetic resonance imaging method for imaging an anatomical region of a subject, the method comprising: generating an imaging field, the anatomical region being provided in an acquisition space within the imaging field; generating multiple acquisition sequences, each acquisition sequence including an RF excitation pulse, and gradient field pulses configured to generate a readout trajectory in *k*-space, each readout trajectory including a number of scan lines extending in a frequency encoding direction and spaced in a second phase encoding direction along a phase encoding axis, and the multiple acquisition sequences generating a plurality of readout trajectories extending over at least part of an acquisition space, the readout trajectories being rotated at least partially about the phase encoding axis; acquiring echo signals from the readout trajectories for each of the multiple acquisition sequences to generate *k*-space data; and, processing the *k*-space data to generate at least one image representation of the anatomical region.

[0009] In one embodiment, the method includes undersampling in at least one of a radial and a phase encoding direction.

[0010] In one embodiment, the readout trajectories are undersampled with an undersampling factor of $R_{PE} > 1$ to shorten echo signal acquisition times.

[0011] In one embodiment, the method includes undersampling to acquire echo signals from selected scan lines of a trajectory, thereby missing at least some scan lines.

[0012] In one embodiment, the method includes acquiring echo signals from missing scan lines in subsequent acquisitions.

[0013] In one embodiment, the method includes acquiring echo signals from at least one of: interleaved scan lines of multiple trajectories; and, block-wise segmented trajectories.

[0014] In one embodiment, the method includes performing accelerated imaging by reconstructing data from missing scan lines.

[0015] In one embodiment, the method includes reconstructing data using at least one of: echo signals acquired from different scan lines in the trajectory; echo signals acquired from scan lines of different trajectories; echo signals acquired from scan lines of adjacent trajectories; echo signals acquired from equivalent different scan lines of adjacent trajectories and, echo signals acquired from different scan lines of adjacent trajectories.

[0016] In one embodiment, the method includes sampling at least one common scan line in two different readout trajectories with different echo times.

[0017] In one embodiment, the multiple readout trajectories are asymmetrically arranged with respect to the phase encoding axis.

[0018] In one embodiment, the degree of asymmetry changes during acquisition.

[0019] In one embodiment, the method includes applying multiple acquisition sequences to generate a homogeneous azimuthal distribution of readout trajectories.

[0020] In one embodiment, the readout trajectories are distributed by an azimuthal angle Θ given by:

$$\Theta_j = \frac{(j-1)2\pi}{N} + \vartheta(j)$$

where: N denotes the number of trajectories

$$\vartheta(j) = \begin{cases} 0 & f \quad 1 \leq j \leq N/2 \\ \pi/N[(N-1)m \quad 2] & f \quad N/2 < j \leq N \end{cases}$$

[0021] In one embodiment, the method includes generating readout trajectories spaced by a golden angle.

[0022] In one embodiment, the method includes generating readout trajectories spaced by an azimuthal angle according to:

$$\Delta\Theta = {}^{\pi}/_{(1+\sqrt{5})/2 + Q - 1}$$

where Q can be any integer number.

[0023] In one embodiment, the method includes generating readout trajectories spaced by a random azimuthal angle increment.

[0024] In one embodiment, the readout trajectory is rotated about the phase encoding axis as the phase encoded signals are acquired to define a curved readout trajectory.

[0025] In one embodiment, the phase encoding axis is orientated at least one of: along a shortest dimension of the anatomical region; perpendicular to a trajectory of the at least one image representation; and, perpendicular to a transverse trajectory of the subject.

[0026] In one embodiment, a variation of the azimuthal angle of the readout trajectory is defined by a variation of the amplitude of pulses in readout gradient fields.

[0027] In one embodiment, an asymmetry about a phase encoding axis is controlled based on an amplitude of dephaser pulses in readout gradient fields.

[0028] In one embodiment, at least one acquisition sequence includes at least one of: an RF excitation pulse; and, a preparation module including one or more pulses.

[0029] In one embodiment, the method of reconstructing data includes at least one of: performing phase correction; at least one of: combining echo signals from multiple trajectories; and, reconstructing missing data from undersampled trajectories; performing a Fourier transform along a phase encoding axis; regridding to a uniform grid; and, combining individual data subsets into a combined dataset.

[0030] In one embodiment the method of reconstructing data includes exploiting the symmetry of *k*-space.

[0031] In one embodiment the method of acquiring and reconstructing data uses a partial Fourier techniques.

[0032] In one embodiment the method of reconstructing includes filtering of *k*-space data.

[0033] In one embodiment the method of reconstructing uses at least one of: prior knowledge; prior knowledge of different echo-times of individual trajectories; prior knowledge of contrasts of individual trajectories; and, a model-based reconstruction.

[0034] In one embodiment, the method includes processing the *k*-space data by interpolating echo signals onto equidistant sampling points along a readout axis to remove non-linearities.

[0035] In one embodiment, the method includes processing the *k*-space data by performing, for echo signals from at least one readout trajectory, at least one of: gradient delay; Nyquist ghost correction; physiologic noise correction; and, eddy current corrections.

[0036] In one embodiment, the method includes processing the *k*-space data by: acquiring one or more non-phase-encoded navigator echo signals between each RF excitation and acquiring echo signals from the readout trajectories; estimating a gradient delay induced shift along a readout axis; and, correcting for gradient delays using the estimated gradient delay.

[0037] In one embodiment, the method includes processing the *k*-space data by: obtaining shifts at multiple azimuthal readout trajectory angles; fitting shift values to a gradient delay model; and, using delay model fit values to correct for the linear phase errors between the odd and even scan lines.

[0038] In one embodiment, the method includes processing the *k*-space data for at least one of susceptibility mapping and relaxation time mapping.

[0039] In one broad form an aspect of the present invention seeks to provide a magnetic resonance imaging apparatus for imaging an anatomical region of a subject, the apparatus comprising: a magnetic resonance imaging device; and, one or more processing devices that: control the magnetic resonance imaging device to cause the magnetic resonance imaging device to: generate an imaging field, the anatomical region being provided in an acquisition space in the imaging field; generate multiple acquisition sequences, each acquisition sequence including an RF excitation pulse, and gradient field pulses configured to generate a readout trajectory in *k*-space, each readout trajectory including a number of scan lines extending in a frequency encoding direction and spaced in a second phase encoding direction

along a phase encoding axis, and the multiple acquisition sequences generating a plurality of readout trajectories extending over at least part of the acquisition space, the readout trajectories being rotated at least partially about the phase encoding axis; acquire echo signals from the readout trajectories for each of the multiple acquisition sequences to generate *k*-space data; and, process the *k*-space data to generate at least one image representation of the anatomical region.

[0040] In one broad form an aspect of the present invention seeks to provide a magnetic resonance imaging method for imaging an anatomical region of a subject, the method comprising: generating an imaging field, the anatomical region being provided in an acquisition space in the imaging field; generating multiple acquisition sequences, each acquisition sequence including an RF excitation pulse, and gradient field pulses configured to generate a readout trajectory in *k*-space, each readout trajectory including a number of scan lines extending in a frequency encoding direction and spaced in a second phase encoding direction along a phase encoding axis, and the multiple acquisition sequences generating a plurality of readout trajectories extending over at least part of the acquisition space, wherein at least one of the acquisition sequences is undersampled in at least one of a frequency and a phase encoding direction; acquiring echo signals from the multiple readout sub-trajectories for each of the multiple acquisition sequences to generate *k*-space data including reconstructed readout trajectories; and, processing the *k*-space data to generate at least one image representation of the anatomical region.

[0041] In one broad form an aspect of the present invention seeks to provide a magnetic resonance imaging apparatus for imaging an anatomical region of a subject, the apparatus comprising: a magnetic resonance imaging device; and, one or more processing devices that: control the magnetic resonance imaging device to cause the magnetic resonance imaging device to: generate an imaging field, the anatomical region being provided in an acquisition space in the imaging field; generate multiple acquisition sequences, each acquisition sequence including an RF excitation pulse, and gradient field pulses configured to generate a readout trajectory in *k*-space, each readout trajectory including a number of scan lines extending in a frequency encoding direction and spaced in a second phase encoding direction

along a phase encoding axis, and the multiple acquisition sequences generating a plurality of readout trajectories extending over at least part of the acquisition space, wherein at least one of the acquisition sequences is undersampled in at least one of a frequency and phase encoding direction; acquire echo signals from the multiple readout sub-trajectories for each of the multiple acquisition sequences to generate *k*-space data including reconstructed readout trajectories; and, process the *k*-space data to generate at least one image representation of the anatomical region.

[0042] It will be appreciated that the broad forms of the invention and their respective features can be used in conjunction, interchangeably and/or independently, and reference to separate broad forms is not intended to be limiting.

Brief Description of the Drawings

[0043] Various examples and embodiments of the present invention will now be described with reference to the accompanying drawings, in which: -

[0044] Figure 1A is a schematic diagram of an example of an imaging apparatus;

[0045] Figure 1B is a schematic diagram of an example of a processing system;

[0046] Figure 2 is a flow chart of an example of an image generation process;

[0047] Figure 3 is a schematic diagram of an example of an acquisition pulse sequence;

[0048] Figure 4A is a schematic diagram of an example of a readout trajectory;

[0049] Figure 4B is a schematic diagram showing a perspective view of an example of a rotating EPI readout trajectory arrangement;

[0050] Figure 4C is a schematic diagram showing a plan view of the rotating EPI readout trajectory arrangement of Figure 4B;

[0051] Figure 4D is a schematic diagram of a perspective view of an example of an asymmetric rotating EPI readout trajectory arrangement;

[0052] Figure 4E is a schematic diagram of a plan view of the asymmetric rotating EPI readout trajectory arrangement of Figure 4D;

[0053] Figures 5A and 5B are positive and negative images reconstructed from an *in vivo* 3D rotating EPI dataset;

[0054] Figures 6A and 6B are positive and negative images reconstructed from 3D multi-echo GRE measurement and a first repetition of the threefold segmented 3D rotating EPI measurement;

[0055] Figures 7A and 7B are positive and negative images illustrating geometric distortion and effects of averaging and acceleration in the 3D rotating EPI data;

[0056] Figure 8 shows susceptibility maps obtained from the 3D GRE and the first 3D rotating EPI measurements;

[0057] Figure 9 shows graphs of susceptibility values (mean and standard deviation) measured within the caudate, pallidum, putamen and corpus callosum of one volunteer

[0058] Figure 10 shows graphs of susceptibility measured with 3D rotating EPI as a function of the susceptibility obtained using 3D GRE;

[0059] Figures 11A and 11B are positive and negative images showing the effects of motion observed for the threefold segmented 3D rotating EPI measurement;

[0060] Figure 11C is a graph showing a calculated susceptibility within the pallidum plotted against the overall acquisition time;

[0061] Figures 12A and 12B are positive and negative images of 3D rotating EPI and 3D rotating asymmetric EPI; and,

[0062] Figure 13 is an image showing a comparison between the resolution of small anatomical features 3D rotating EPI and 3D rotating asymmetric EPI.

Detailed Description of the Preferred Embodiments

[0063] An example of a MRI system will now be described with reference to Figure 1A.

[0064] For the purpose of this example, the MRI system 100 includes a main or primary shimmed magnet 101, three principal axis gradient coils 102, a patient/sample bed 108 and MR instrumentation 109. In use, the main magnet 101 is adapted to generate a substantially homogeneous static magnetic imaging field B_0, whilst the gradient coils apply gradient fields G_x, G_y, G_z, over an acquisition space 111, which contains a subject, such as at least part of a patient or sample. The subject is also exposed to an RF field, generated by an RF coil (not shown) allowing MRI to be performed. The workings of these components are substantially identical to those of contemporary systems, and will not therefore be described in any further detail.

[0065] In one example, the above described process is performed at least in part utilising a processing system, which may be coupled to, or form part of, the MR instrumentation 109. An example processing system will now be described with reference to Figure 1B.

[0066] In this example the processing system 120 includes a processor 121, a memory 122, an input/output device, such as a keyboard and mouse 123, and an optional external interface 124 coupled together via a bus 125. The optional external interface may be coupled to a database 126, allowing the processing system 120 to store data and/or access previously stored data.

[0067] In use, the processor 121 typically executes applications software stored in the memory 122, to allow the processor 121 to control the MRI system, perform required calculations and/or display results. This can include, for example, performing analysis of the imaging field and collected sample data in order to generate image data, as well as optionally to assist in generating transform functions. It will be appreciated that these processes can be performed automatically, but typically involve at least some input or other control by the user.

[0068] It will therefore be appreciated that the processing system 120 may be one or more suitably programmed computer systems, such as a desktop and/or server, or the like, although alternatively the processing system 120 may be formed from specialised hardware forming part of the MRI system.

[0069] An example of a process for generating an image using magnetic imaging will now be described with reference to Figure 2.

[0070] At step 200 the MRI system is used to generate an imaging field B_0, with the anatomical region of the subject being provided in the acquisition space and hence in the imaging field.

[0071] At step 210, multiple acquisition sequences are generated. As shown in Figure 3, each acquisition sequence includes an RF excitation pulse 300, and encoding gradient field pulses G_x, G_y, G_z 302, which are applied to the anatomical region of the subject in the acquisition space.

[0072] Each pulse sequence is configured to generate a readout trajectory in k-space, with each readout trajectory including a number of scan lines extending in a frequency encoding direction and spaced in a second phase encoding direction along a phase encoding axis.

[0073] An example of a planar readout trajectory is shown in Figure 4A, with the frequency encoding direction corresponding to k_x for this orientation of the planar trajectory, and the phase encoding direction k_y, with the phase encoding axis being shown at 401. It will be appreciated however that readout trajectories having other shapes could be used, including but not limited to: helical, staircase, random, star, curved, spiral, cork-screw, cylindrical, or the like. The following examples will focus on the use of a planar trajectory, but it will be appreciated that this is not intended to be limiting.

[0074] The multiple acquisition sequences are configured so as generate a plurality of readout trajectories extending over at least part of the acquisition space, the readout trajectories being rotated about the phase encoding axis 401, as shown in Figures 4B and 4C. In this regard, an azimuthal angle of the readout trajectory can be controlled by adjusting the

relative amplitude of pulses in readout gradient fields G_x, G_z. Whilst rotation is only about the phase encoding axis in this example, it will be appreciated that rotation could also be performed about other axes, as long as at least a component of the rotation is about the phase encoding axis.

[0075] In a further example, which will be described in more detail below, the readout trajectory can be generated asymmetrically arranged with respect to the phase encoding axis, so that the trajectory is offset in the frequency encoding direction, to thereby acquire higher frequencies during the acquisition, although this is not essential.

[0076] Echo signals are acquired for each of the acquisition signals at step 220, allowing *k*-space data to be obtained. This is typically performed synchronously with the gradient pulses G_x, G_z, as shown by the pulses ADC in Figure 3, which refer to the acquisition of MRI signal by an analog-to-digital converter (ADC) forming part of the MRI system.

[0077] This process is performed multiple times using respective acquisition sequences, with the resulting *k*-space data being used to construct at least one image representation of the anatomical region image at step 230, which can be performed using known processing techniques.

[0078] Accordingly, the above described process uses an echo imaging type approach in which readout trajectories are rotated about a phase encoding axis in order to generate images of the anatomical region. This approach has a number of benefits over more traditional Cartesian based approaches. In particular, this provides greater coverage about the phase encoding axis in *k*-space, which helps improve the contrast of the acquired images. This in turn allows data to be collected more rapidly, whilst maintaining a good signal-to-noise ratio. For example, the technique can be used to provide mapping at an isotropic resolution of 1mm with a sufficiently high image quality and signal-to-noise ratio in the phase data to allow it to be used for reliable QSM processing.

[0079] Additionally, the approach can easily be utilised with various undersampling and accelerated imaging protocols, as will be described in more detail below, thereby further reducing image acquisition time. Such rapid image acquisition is particularly suited for

whole brain susceptibility mapping, as the reduction in imaging time helps minimise subject movement during imaging. It will be appreciated however that the imaging methodology can also have applicability to a wide range of other applications including, but not limited to: *T2** weighted imaging, Susceptibility Weighted Imaging (SWI), QSM, Arterial Spin Labelling (ASL), functional MRI (fMRI), or the like. The readout can also be used for *T2* weighted imaging by including a 180° RF refocussing pulse as part of a spin echo preparation module, whilst RF preparation modules can be added to enable fast *T1*-mapping, Magnetisation Transfer (MT) contrast imaging, or the like.

[0080] A number of further features will now be described.

[0081] In one example, the method includes undersampling in at least one of a radial and an axial direction, by omitting trajectories or scan lines within individual trajectories or a combination of both. In general, this can be used to reduce the length of time over which data is collected, which in turn can help reduce movement artefacts. In addition, undersampling the readout trajectories with an undersampling factor of $R_{PE} > 1$ can be used to shorten echo times and reduce signal decay artefacts.

[0082] When undersampling along the phase encoding axis, this can involve acquiring echo signals from selected scan lines of a trajectory, thereby missing at least some scan lines, for example by acquiring data from every second or third scan line or by skipping a whole block of scan lines.

[0083] Data from missing scan lines can then be collected using subsequent acquisitions, for example by interleaving scan lines of different trajectories. In this example, multiple readout trajectories at a given azimuthal position could be used in order to collect data over a complete set of scan lines. This is often referred to as segmentation. It will be appreciated that other segmentation strategies could also be used, such as block-wise segmented trajectories, with all scan lines in a first block being collected separately from all scan lines in a subsequent block, at the same azimuthal angle. In a further example, the readout trajectories can be configured to overlap so that at least some scan lines are sampled with different echo times. So for example, this could involve acquiring echo signals from scan

lines 1-21 for a first sub-trajectory, and then lines 20-40 for a subsequent trajectory, so that lines 20-21 are sampled twice at different echo times. This can assist in image reconstruction, and help avoid artefacts caused by signal drop-out or the like.

[0084] As an alternative to collecting data from missing scan lines over multiple acquisitions, the method could include performing accelerated imaging by exploiting symmetry of the echo signals in *k*-space. The concept, widely known as partial Fourier, skips echo signals from up to half of a readout trajectory, in turn allowing the acquisition to be performed faster, in turn potentially allowing to reduce the echo-time. In the image reconstruction, the skipped lines can then be filled with zero values or specific partial Fourier reconstruction techniques can be employed.

[0085] As another alternative to collecting data from missing scan lines (including missing trajectories) over multiple acquisitions, the method could include performing accelerated imaging by reconstructing data from missing scan lines. In this instance, data could be reconstructed based on echo signals acquired from different scan lines in the same trajectory, or from scan lines in different trajectories, or both. The different trajectories would typically be adjacent trajectories, although this is not essential, and extrapolation from non-adjacent trajectories could be performed. When using data from adjacent trajectories, the reconstruction can use echo signals acquired from different scan lines of adjacent trajectories, so that for example, the reconstruction of scan line 6 of a first trajectory uses echo signals acquired from scan line 5 of a second trajectory. Alternatively, reconstruction can be performed using echo signals acquired from equivalent scan lines, so that for example, the reconstruction of scan line 6 of a first trajectory uses echo signals acquired from scan line 6 of a second trajectory. In another example, acquisition skips scan lines during the measurement, with the undersampling patterns being interleaved in adjacent readout trajectories. For example, the approach skips scan lines 2, 4, 6, ... in first, third, fifth,... readout trajectories and scan lines 1, 3, 5,... in the second, fourth, sixth... readout trajectories. This can significantly improve the image reconstruction, while minimising acquisition time. It will also be appreciated that the concept is not limited to an acceleration

factor of 2, but rather any number of scan lines could be skipped, with data being reconstructed from one or more adjacent trajectories as needed.

[0086] It will be appreciated that other reconstruction techniques can be used in addition to, or as an alternative to those described above. For example, reconstruction can be performed taking into account prior knowledge, such as knowledge of sample response or image properties (e.g. sparsity in transform domains), as well performing reconstruction in image space as opposed to *k*-space.

[0087] In one particular example, reconstruction involves obtaining echo signals and using *k*-space filtering or model-based reconstructions including prior knowledge, to allow images or tissue specific parameters (relaxation times, susceptibility or the like) to be derived from either a single acquisition, or one or more partial or fully sampled acquisitions.

[0088] In this regard, *k*-space filtering takes into account the fact that the contrast information of an image is stored in the centre of *k*-space, while the resolution information is found in its outer parts. Using the above described rotational acquisition scheme means that the centre of *k*-space is regularly sampled, and so it is possible to filter *k*-space before the reconstruction, so that specific scan lines carrying specific contrast information are weighted higher than other lines.

[0089] Using an acquisition that incorporates trajectories with different echo-times or contrast information, allows certain trajectories with a specific echo-time or contrast to be given a higher weighting than other trajectories in the *k*-space centre. It will also be possible to only use the information of a single trajectory in the centre of *k*-space to constrain the echo-time or contrast of the reconstruction, with information from other trajectories being used to obtain information about the spatial resolution. A reconstruction like this can, for example, be used to obtain images with different echo-times or contrasts from less than one acquisition for each echo-time or contrast. It will be appreciated that this can reduce the amount of sampling required, which in turn can reduce imaging time.

[0090] Instead or in addition to *k*-space filtering, it is also possible to incorporate prior knowledge on different echo-times or contrasts of individual trajectories in the reconstruction

or to use a model-based reconstruction. If for example, a-priori information about the contrast at the time of acquisition of a trajectory is known or the contrast is given by a certain signal behaviour, such as an exponential decay, incorporating a model of this decay into the reconstruction (e.g. an iterative optimization), enables the parameters that describe the signal decay (e.g. one or more tissue specific parameters) to be determined for each pixel. In addition to this, it can be possible to obtain the images at different echo-times or contrasts from this reconstruction.

[0091] In another example, echo-time shifting can be performed while rotating the readout trajectories. In effect this involves not only rotating the readout trajectories about the phase encoding axis, but also shifting them along the phase encoding axis. For example, from a first readout trajectory scan lines 1-40 could be sampled, whilst in subsequent trajectories, scan lines 2-41, 3-42, and the like can be sampled. Again, the echo will always occur in line 21, but the time that passes between excitation and echo formation will differ in every trajectory, again helping to avoid signal drop-out artefacts, or the like. In practice this could be achieved by adjusting a dephaser pulse for the phase encoding field G_y for the different readout trajectories.

[0092] As previously mentioned, in one example, the multiple readout trajectories are asymmetrically arranged with respect to the phase encoding axis to acquire higher spatial frequencies during the acquisition, or to reduce the scan and echo-time while maintaining spatial resolution, as shown for example in Figures 4D and 4E. In this example, the asymmetry is controlled based on an amplitude of dephaser pulses in readout gradient fields G_x, G_z. In a further example, the degree of asymmetry can change during acquisition, thereby providing an effective elliptical or partial coverage of *k*-space.

[0093] The acquisition sequences are typically configured to generate a homogeneous azimuthal distribution of readout trajectories. Whilst it will be appreciated that a range of different readout trajectory arrangements could be used, in one example, the trajectories are spaced so that over 360°, readout trajectories are interleaved as shown in Figure 4C. In this example, the readout trajectories are distributed by an azimuthal angle Θ given by:

$$\Theta_j = \frac{(j-1)2\pi}{N} + \vartheta(j)$$

where: N denotes the number of trajectories

$$\vartheta(j) = \begin{cases} 0 & f \quad 1 \leq j \leq N/2 \\ \pi/N[(N-1)m \quad 2]f & N/2 < j \leq N \end{cases}$$

[0094] The approach can use readout trajectories spaced by any suitable angle $\Delta\Theta$. This includes randomly chosen angle increments, but in one example this is a golden angle or tiny golden angle, given by

$$\Delta\Theta = {}^{\pi}/_{(1+\sqrt{5})/2 + Q - 1}$$

where Q can be any integer number.

[0095] This for example corresponds to an azimuthal angle increment of at least one of approximately 111.2° (Q = 1), approximately 68.8° (Q = 2) approximately 49.8° (Q = 3), approximately 39.0° (Q = 4), approximately 32.0° (Q = 5), approximately 27.2° (Q = 6), or approximately 23.6 (Q = 7). Such arrangements achieve a very uniform coverage of the 3D cylindrical volume with a small number of trajectories, which is particularly advantageous for time-resolved measurements, such as functional MRI. A random readout trajectory acquisition order can also be used, thereby effectively selecting or increasing the azimuthal angle randomly, which can be used to avoid the need to use spoiler gradient fields. In this regard, spoiler gradient fields are normally used to dephase and remove magnetization after the acquisition of a readout trajectory is finished, thereby removing artefacts in the image. However, using a random scheme allows the spoiling gradient field to be avoided, thereby shortening the acquisition time for each trajectory and reducing potential eddy-current effects.

[0096] It will also be appreciated that other arrangements could be used, such as rotating the readout trajectory about the phase encoding axis as the phase encoded signals are acquired to define a curved readout trajectory.

[0097] In one example, the phase encoding axis is orientated along a shortest dimension of the anatomical region, perpendicular to a trajectory of the at least one image representation or perpendicular to a transverse trajectory of the subject. In particular, orientating the phase encoding axis along a shortest dimension of the anatomical region, for example perpendicular to the transverse trajectory of the subject when brain imaging, can minimise the time taken to acquire data from a readout trajectory, in turn reducing the echo-time and the acquisition bandwidth along the phase encoding axis, which can help reduce distortions and signal dropouts. Additionally, by orientating the phase encoding axis perpendicularly to the image plane of the images to be displayed, this means that distortions arising within the trajectory are less pronounced as the readout trajectory is oriented perpendicular to the image plane.

[0098] The image reconstruction process will vary depending on the particular approach used. Typically this will involve one or more of the following steps: performing phase correction; either combining echo signals from multiple undersampled trajectories or reconstructing missing data from undersampled trajectories; performing a Fourier transform along a phase encoding axis; regridding to a uniform grid; and, combining individual data subsets into a combined dataset.

[0099] In one example, the method of processing the *k*-space data includes interpolating echo signals onto equidistant sampling points along a readout axis to remove non-linearities and specifically ramp sampling induced non-linearities. The method can also include processing the *k*-space data by performing any one or more of gradient delay, Nyquist ghost correction, physiologic noise correction, eddy current corrections, measuring the trajectory, or the like, for echo signals from each readout trajectory.

[0100] In one example, the method includes processing the *k*-space data by acquiring optional non-phase-encoded navigator echo signals between each RF excitation and acquiring echo signals from the readout trajectories, as shown at 301 in Figure 3. A gradient delay induced shift along a readout axis is then estimated, for example using an average delay between the first and third and the second navigator echo signals or any other suitable approach, with this being used to correct for gradient delays using the estimated gradient delay. Alternatively, however, the navigator pulses could be omitted, with the radial

symmetry being used to correct for gradient delays, which would shorten the echo time and reduce the acquisition time for each trajectory.

[0101] In another example, the method includes processing the *k*-space data by obtaining shifts at multiple azimuthal readout trajectory angles, fitting shift values to a gradient delay model and using delay model fit values to correct for the linear phase errors between the odd and even scan lines.

[0102] When used for phase imaging, susceptibility weighted imaging, or susceptibility mapping, known processing techniques can be used, which may include determining phase data for each coil channel individually, deriving a brain mask from combined magnitude data and obtaining susceptibility mapping images by calculating the mean of all channels, although channels could be combined initially depending on the preferred approach.

[0103] Similarly, appropriate acquisition and reconstruction techniques could be used for other applications, such as relaxation time mapping. For example, employing a staircase trajectory, in which azimuthal rotation occurs as the trajectory progresses along the phase encoding axis, together with a model-based reconstruction, can be used to estimate *T2** relaxation times from one or more acquisitions.

[0104] The above described techniques and in particular the accelerated acquisition techniques and perpendicular orientation of the phase encoding axis relative to the image plane and/or shortest anatomical axis, can also be used with Cartesian acquisition schemes, for example in which readout trajectories are provided in a parallel arrangement spaced in a direction perpendicular to the phase encoding axis.

[0105] In this example, the magnetic resonance imaging method comprises generating an imaging field, the anatomical region being provided in the imaging field; generating multiple acquisition sequences, each acquisition sequence including an RF excitation pulse, and phase encoding gradient field pulses configured to generate a readout trajectory in *k*-space, each readout trajectory including a number of scan lines extending in a frequency encoding direction and spaced in a second phase encoding direction along a phase encoding axis, and the multiple acquisition sequences generating a plurality of readout trajectories extending

over at least part of the acquisition space, wherein the acquisition sequences are undersampled in at least one of a frequency and phase encoding direction; echo signals from the multiple readout sub-trajectories for each of the multiple acquisition sequences to generate *k*-space data including reconstructed readout trajectories; and, processing the *k*-space data to generate at least one image representation of the anatomical region.

[0106] In this example, typically accelerated acquisition techniques include the selection of the orientation of the phase encoding axis relative to the subject, the use of interleaved or segmented readout trajectories, or the like.

[0107] A specific example or a rotational EPI scheme will now be described in further detail.

[0108] In this example, segmented as well as accelerated EPI readout (high sampling efficiency) schemes are combined with the beneficial properties of radial acquisitions (minimal distortion in radial direction, motion robustness) using a non-Cartesian 3D rotating EPI sequence with a paddlewheel shaped readout scheme for QSM at ultra-high field. The so-called planes-on-a-paddlewheel (POP) acquisition scheme is realized by rotating two-dimensional (2D) EPI readout trajectories about the phase encoding axis, which lends itself to the use of advanced undersampling patterns and acceleration techniques.

[0109] To demonstrate the effectiveness of this configuration, measurements were performed using a 7 T whole body MRI scanner (Magnetom 7 T, Siemens Healthcare, Erlangen, Germany) equipped with a SC72 gradient system providing a maximum gradient strength of 70 mT/m and a slew rate of 200 T/m/s. A 7 T Tx/32-channel Rx head array (Nova Medical, Wilmington, MA, USA) was used for RF transmission and signal reception. To improve the B_0 field homogeneity, third order shimming was employed. For the human *in vivo* experiments written informed consent was obtained.

[0110] A 3D EPI sequence was equipped with a POP readout scheme sampling a cylinder shaped *k*-space. As displayed in Figure 4A and 4B, the 3D POP scheme consists of multiple standard 2D EPI readout trajectories rotating about the phase encoding axis. Per excitation a single trajectory on this paddlewheel is sampled, with the 3D slab selective excitation performed along the rotation/phase encoding axis. In this example, segmentation or regular

undersampling is used to allow a reduction of the echo train length. A segmentation or acceleration factor of $R_{PE} = 3$ is being used for illustration. Segments are selected along the phase encoding direction.

[0111] The azimuthal acquisition order used is shown in Figure 4C, with the numbers indicating the order of sampling. The azimuthal angle Θ is constantly increased within [0; 2π]. For even projection numbers, the second half of the projections are interleaved between the first half.

[0112] The azimuthal angle Θ of the jth trajectory is thereby calculated as:

$$\Theta_j = \frac{(j-1)2\pi}{N} + \vartheta(j)$$

where: N denotes the number of trajectories

$$\vartheta(j) = \begin{cases} 0 & f \quad 1 \leq j \leq N/2 \\ \pi/N[(N-1)m \quad 2]\, f & N/2 < j \leq N \end{cases}$$

[0113] This ensures correct interleaving for even numbers of trajectories, which can allow for an improved gradient delay correction.

[0114] To evaluate the performance of the 3D POP EPI sequence for QSM, *in vivo* brain imaging was performed in three healthy volunteers.

[0115] Three basic protocols with three different echo times were set up by employing three different partial Fourier factors (PFs), and images were obtained at an isotropic resolution of 1 mm using the following acquisition parameters:

- field of view (FOV) = 212 × 212 × 108 mm^3,
- 330 projections (azimuthal angles), PF = 5/8, 6/8, 7/8,
- repetition time (T_R) = 35 ms, 39 ms, 44 ms,
- echo time (T_E) = 12 ms, 16 ms, 21 ms,
- echo spacing (ES) = 1.0 ms,
- flip angle = 11°, 12°, 13°.

[0116] Data sampling was performed with a readout bandwidth (BW_{RO}) of 1180 Hz/pixel incorporating ramp sampling. A 3.2 ms water excitation RF pulse with a bandwidth–time

product of $BWT_{Tx} = 25$ was employed for spin excitation and slab selection. To facilitate the correction of gradient delays and to reduce Nyquist ghosting, three non-phase-encoded navigator echoes were acquired between each RF excitation and EPI readout.

[0117] To achieve the echo times stated above and to minimize geometric distortions, *k*-space was segmented by a factor of $R_{PE} = 3$ along the phase encoding direction, yielding effective echo train lengths of 35, 39 and 44 for the three different echo times. To mitigate potential influences of physiological effects, the *k*-space for each trajectory was fully covered using three interleaved shots before incrementing the azimuthal angle. Acquisition times per volume were 35 s, 39 s and 43 s. Repeating the measurements nine, nine and eight times resulted in overall acquisition times of 312 s, 347 s and 349 s, respectively.

[0118] In addition to this, measurements were made with the $T_E = 16$ ms (PF = 6/8) protocol employing parallel imaging with an undersampling factor of $R_{PE} = 3$ instead of *k*-space segmentation along the phase encoding direction. A temporal GRAPPA (TGRAPPA)-like sampling scheme was employed to facilitate the image reconstruction from the acquired data itself. Keeping all other acquisition parameters unchanged, the protocol allows coverage of a threefold undersampled *k*-space within 13 s.

[0119] For comparison, brain imaging was performed using a 3D multi-echo GRE sequence. Again, the images were acquired at an isotropic spatial resolution of 1 mm^3. The acquisition parameters included:

- FOV = 212 × 212 × 120 mm^3,
- 104 partitions,
- slice oversampling = 15.4%,
- $T_R = 29$ ms,
- 7 echoes, first echo time (T_{E1}) = 4.36 ms,
- ES = 2.86 ms,
- flip angle =13°,
- $BW_{RO} = 600$ Hz/pixel.

[0120] Parallel imaging was applied along the phase encoding direction with an acceleration factor of $R_{PE} = 3$ and 24 auto-calibration lines additionally acquired for image reconstruction.

[0121] For both the 3D POP EPI and the 3D GRE measurements, slab selection was performed along the same axis. Consequently, the phase encoding direction of the 3D POP EPI measurements matched the partition encoding direction of the 3D GRE scan. Slices positioned perpendicular to this axis (x–z plane) will be referred to as "axial", and slices positioned parallel to the x–y and y–z planes as "coronal" and "sagittal", respectively.

[0122] Image reconstruction for the 3D POP EPI data was performed using MATLAB (MathWorks, Natick, MA, USA). First, all ramp-sampling induced non-linearities along the readout axis were removed by interpolating the data onto equidistant sampling points. Hereafter, a gradient delay and Nyquist ghost correction was performed: for each trajectory, the gradient delay induced shift along the readout axis was estimated using known techniques based on an average of the first and third and the second navigator as the two opposed calibration lines. To minimize the influence of noise and eddy currents in the estimation, the shifts obtained at all angles Θ were fitted using the appropriate gradient delay model.

[0123] The fit values were finally used to correct for the linear phase errors between the odd and even phase encoding lines. The phase correction was carried out individually for each acquired data subset, i.e. before combining individual segments into a measurement or reference dataset. If required, GRAPPA was employed to reconstruct the missing phase encoding lines with the weight sets determined trajectory-wise from the combined acquired data subsets. After zero-filling and applying the Fourier transform along the phase encoding direction, the non-Cartesian data of each axial slice was reconstructed using non-uniform fast Fourier transform (NUFFT) software. Finally, the multiple receiver channels were combined by calculating the root sum of squares.

[0124] The images for the 3D GRE measurement were calculated online using the reconstruction pipeline provided by the manufacturer. For the parallel imaging reconstruction GRAPPA was utilized with 36 auto-calibration lines for weight set calculation. Again, a root-sum-of-squares receiver channel combination was employed to finalize the reconstruction.

[0125] For susceptibility mapping, the image phase was extracted from the uncombined single-channel data and processed using a total generalized variation (TGV) method. The mapping procedure incorporates phase unwrapping, background field removal and dipole inversion in a single step. The required brain mask was generated based on root-sum-of-squares-combined magnitude data using the segmentation and image calculator module of SPM12 (Wellcome Trust Centre for Neuroimaging, London, UK). To ensure comparability between all 3D POP EPI and the 3D GRE protocols, the mask was obtained from the 3D POP EPI dataset with $T_E = 21$ ms and used for processing all 3D POP EPI and 3D GRE data. The single-channel susceptibility maps were finally combined by computing the mean across all channels.

[0126] The susceptibility maps calculated from Echoes 4, 5 and 7 ($T_E = 12.9$ ms, 15.8 ms and 21.5 ms) of the 3D GRE measurement were extracted for comparison with corresponding 3D POP EPI based susceptibility maps ($T_E = 12$ ms, 16 ms and 21 ms). For the 3D POP EPI approach, each measurement was processed independently, yielding an individual susceptibility map for each repetition. For post-processing, the maps were motion corrected with respect to each other using the Oxford FMRIB Software Library (FSL) MCFLIRT toolbox.

[0127] Effects of the gradient delay and Nyquist ghost correction were assessed by comparing the images obtained using the new EPI acquisition scheme with images reconstructed from the same data without applying the phase correction. Single volume and *k*-space averaged multi-repetition images were also compared with corresponding images reconstructed from the 3D GRE data. To assess geometric distortions, the reconstructed images were co-registered using FMRIB's Linear Image Registration Tool (FLIRT) with six degrees of freedom, and subsequently tissue boundaries were extracted from the GRE images using an edge detection algorithm in MATLAB (MathWorks) and overlaid on the POP EPI data. Visual comparisons were also made for the QSM images obtained using the two different sequences. A detailed analysis was performed on the susceptibilities measured within the corpus callosum and the three iron-rich sub-cortical structures, caudate, putamen

and pallidum. All anatomical regions were manually outlined in susceptibility maps using the ITK-SNAP software.

[0128] Effects of the gradient delay and Nyquist ghost correction are displayed in Figures 5A and 5B, where the reconstructions of representative axial and sagittal slices obtained without (left-hand column) and with employing the phase correction (center column) are compared. Images are reconstructed from an *in vivo* 3D POP EPI dataset without (left) and with (middle) Nyquist ghost correction, with the difference between the two reconstructions (right). Apart from removing Nyquist ghosting (arrows 501) the correction improves the signal homogeneity (arrows 502) and has a significant influence on the combination of individual segmentation subsets (arrows 503). For better visibility all difference images were multiplied by a factor of 5.

[0129] The utilization of the phase correction not only removes Nyquist ghost artefacts, it also decreases signal inhomogeneities with low spatial frequencies. Additionally, the combination of individual segmentation subsets significantly benefits from the correction. Similar effects are observed for GRAPPA reconstructed datasets. The improved combination of segmentation subsets in the TGRAPPA calibration data leads to substantially reduced residual undersampling artefacts in the sagittal views.

[0130] Images obtained from the 3D GRE and the first repetition of the 3D POP EPI measurements are displayed in Figures 6A and 6B, on the left and right, respectively. The images are reconstructed from the 3D multi-echo GRE measurement at $T_E = 12.9$ ms, 15.8 ms and 21.5 ms (left) and the first repetition of the threefold segmented 3D POP EPI measurements with $T_E = 12$ ms, 16 ms and 21 ms (right). For each echo time, eight of the 108 reconstructed axial slices are depicted. Echo times, PFs and total acquisition times are given in the images (bottom, left to right).

[0131] As expected for the high spatial resolution, the smaller features of the brain are well depicted and the images are free of significant segmentation and streaking artefacts. Typical EPI signal dropouts are particularly visible in the proximity of the paranasal sinuses, within inferior slices and the cerebellum. As expected, their extent increases with the echo time.

Although providing a lower SNR, the EPI images provide slightly higher contrast. This is particularly visible in the bottom left slice for the measurement with $T_E = 21$ ms. The geometry of the GRE and EPI images compares well.

[0132] Figure 7A and 7B compares images obtained using the different 3D POP EPI protocols with $T_E = 16$ ms and the 3D GRE sequence at $T_E = 15.8$ ms to highlight geometric distortion and effects of averaging and acceleration in the 3D POP EPI data. Representative non-registered views of the axial (top row), coronal (middle) and sagittal (bottom row) planes reconstructed from the 3D GRE dataset at $T_E = 15.8$ ms (left-hand column) and the threefold segmented (seg) 3D POP EPI dataset with $T_E = 16$ ms (center column). The strongest signal boundaries found within the 3D GRE images (left-hand column) were extracted and superimposed as contour lines on top of the single-volume threefold segmented 3D POP EPI images (center column). To allow for a better comparison, an affine co-registration algorithm was applied to the GRE-images before calculating the contours.

[0133] Distortions are only observed along the phase encoding direction. Arrows indicate areas with major geometric distortions. The same axial slice is also depicted for the ninefold *k*-space average (avg) of all 3D POP EPI repetitions (right-hand column, top) as well as the threefold accelerated and GRAPPA reconstructed 3D POP EPI measurement (right-hand column bottom). The overall acquisition time is given in the bottom right of each image.

[0134] Only very small deviations can be identified within the axial plane; increased distortions are found along the *y* axis, as this is the phase encoding direction of the 3D POP EPI scan. The most prominent distortions are depicted by arrows. The *k*-space averaged reconstruction of all threefold segmented 3D POP EPI repetitions (right-hand column, top) shows significantly improved SNR over the single-volume reconstruction (center column). As expected from the short overall acquisition time, the SNR is decreased for the threefold accelerated 3D POP EPI measurement (right-hand column, bottom), resulting in slightly reduced contrast. Substantial non-local signal variations as well as higher order effects of non-linear phase differences are also visible.

[0135] Susceptibility maps obtained from the 3D GRE data at $T_E = 12.9$ ms, 15.8 ms and 21.5 ms (left), and the first repetition of the threefold segmented 3D POP EPI measurements with $T_E = 12$ ms, 16 ms and 21 ms (right) are presented in Figure 8. Echo times, PFs and total acquisition times are given in the images (bottom, left to right). Shown are the same measurements and axial slices as in Figures 6A and 6B. All susceptibility maps were reconstructed using the same regularization parameters for the TGV-QSM algorithm and the same brain mask. In general, the susceptibility maps are highly comparable across the echo times and modalities. Moreover, finer brain structures are similarly well depicted.

[0136] Figure 9 displays susceptibility values (mean and standard deviation) measured within the caudate, pallidum, putamen and corpus callosum of one volunteer using the different non-accelerated segmented 3D POP EPI protocols with $T_E = 12$ ms, 16 ms and 21 ms. The values are plotted against the overall acquisition time of the data included in the evaluation for each region. For comparison, corresponding susceptibility values obtained using the accelerated 3D POP EPI protocol and the 3D GRE sequence are depicted. For each subfigure, the brain region and echo time are given at the top.

[0137] In all four regions, the number of averages basically does not affect the mean or standard deviation. For comparison, the corresponding susceptibilities calculated from the 3D GRE data are depicted as well, and match those measured with the 3D POP EPI approach. Significant differences between the different echo times are not observed. The standard deviation, which represents the variability within a region of interest, is very similar between the 3D GRE and 3D POP EPI measurements.

[0138] Mean susceptibilities and corresponding standard deviations across the individual repetitions of the 3D POP EPI measurements are summarized for all volunteers in Table 1. The standard deviations derived within the corpus callosum and the three sub-cortical structures are typically low, indicating a high reproducibility of the mapping results across repetitions. Slightly higher standard deviations are observed for the third volunteer, particularly within the putamen and pallidum. Here, the mean susceptibility also varies significantly across the different protocols. Larger deviations across the protocols can also be

found for all structures of Subject 2. It is noted that the threefold accelerated 3D POP EPI measurement tends to show the largest deviations compared with the segmented acquisitions.

Table 1

Subject	Measurement	Acquisition time/s	Susceptibility/10^{-3} ppm			
			Caudate	Putamen	Pallidum	Corpus callosum
1	T_E = 12, PF = 5/8	312	26.05 ± 0.15	23.41 ± 0.66	56.51 ± 0.67	−27.8 ± 0.18
	T_E = 16, PF = 6/8	347	28.02 ± 0.24	21.56 ± 0.49	51.36 ± 0.77	−23.48 ± 0.24
	T_E = 21, PF = 7/8	349	29.25 ± 0.19	18.83 ± 0.67	51.06 ± 1.73	−23.28 ± 0.11
	T_E = 16, PF = 6/8, R_{PE} = 3	116	26.62 ± 1.32	20.12 ± 1.83	48.03 ± 2.49	−22.31 ± 2.02
2	T_E = 12, PF = 5/8	312	28.92 ± 0.57	21.99 ± 0.67	76.6 ± 1.04	−28.58 ± 0.23
	T_E = 16, PF = 6/8	347	32.37 ± 0.39	21.62 ± 0.67	74.46 ± 0.69	−21.99 ± 0.29
	T_E = 21, PF = 7/8	349	35.27 ± 0.36	20.45 ± 1.01	67.61 ± 0.75	−16.32 ± 0.33
	T_E = 16, PF = 6/8, R_{PE} = 3	116	28.02 ± 0.92	15.97 ± 1.11	62.16 ± 1.35	−20.2 ± 0.33
3	T_E = 12, PF = 5/8	312	20.19 ± 0.81	0.83 ± 1.9	60.7 ± 5.63	−19.12 ± 0.43
	T_E = 16, PF = 6/8	347	21.6 ± 0.71	−5.77 ± 2.83	89.51 ± 2.56	−21.73 ± 0.29
	T_E = 21, PF = 7/8	349	22.34 ± 0.88	−4.46 ± 2.08	71.27 ± 7.74	−20.51 ± 0.44
	T_E = 16, PF = 6/8, R_{PE} = 3	116	17.57 ± 1.16	2.22 ± 3.26	51.43 ± 2.4	−17.37 ± 0.63

[0139] The generally high reproducibility of the susceptibility values across the protocols can also be seen in Figure 10, which depicts the susceptibility measured with 3D POP EPI as a function of the susceptibility obtained using 3D GRE for three subjects and the different protocols, with a line of identity being given by the dashed line. The Figure shows a generally high correspondence between the different sequences.

[0140] Figures 11A to 11C shows the effects of motion observed for the threefold segmented 3D POP EPI measurement with T_E = 12 ms. Axial slice of the *k*-space averaged reconstruction of all volumes (left-hand image), single-volume reconstructions of Repetition

1 (central image) and Repetition 9 (right-hand image) and calculated susceptibility within the pallidum plotted against the overall acquisition time of the data included in the evaluation (graph, right). Head motion during the acquisition leads to significant blurring and loss of details in the averaged reconstruction and an increasing drift of the calculated susceptibility. The overall acquisition time is given in the bottom right of each image.

[0141] For the medical application of high resolution mapping approaches it is desirable to keep the acquisition time as short as possible, as this greatly reduces the probability of subject motion during acquisition. In the above described arrangement, fast susceptibility mapping is performed at ultra-high field using a non-Cartesian 3D POP EPI acquisition scheme with multiple acquisition protocols. The readout scheme provides significantly shorter acquisition times compared with standard 3D multi-echo GRE imaging with minimal geometric distortions present in the radial plane (x–z), which is particularly important at ultra-high field as the distortion scales linearly with field strength.

[0142] In this context it is noteworthy that minimizing the echo train length and echo time can help reduce geometric distortions or signal dropouts. To obtain a suitable echo time for susceptibility mapping and to reduce distortion also in the phase encoding direction (y), partial Fourier imaging was applied in addition to k-space segmentation. Employing PF = 6/8 enabled whole brain susceptibility mapping at an isotropic resolution of 1 mm in less than 39 s per volume. This temporal footprint could be further reduced to below 13 s using parallel imaging instead of segmentation. An echo time of 16 ms was achieved by employing segmentation or parallel imaging with a factor of $R_{PE} = 3$, and, as demonstrated in Figures 7A and 7B, the major differences in distortions between GRE and POP EPI were within the range of a few pixels.

[0143] Acquiring and averaging data for about 3.5 min, images of comparable quality were obtained using 3D POP EPI and 3D GRE. Evidently, the significantly reduced acquisition times stated above come with a reduction of SNR. While effects are indiscernible for the acquisitions with threefold segmentation, employing an acceleration factor of $R_{PE} = 3$ leads to visible image noise and a reduction of image details. Nevertheless, as can be seen from Figures 9 and 10, and Table 1, even for this accelerated protocol, the 3D POP EPI approach

delivered sufficient SNR within the phase data for the QSM reconstruction. The susceptibilities estimated in the brain and particularly in three iron-rich sub-cortical structures were very similar to those obtained using the 3D multi-echo GRE technique and comparable to previously reported values. This is in line with similar reports that compared EPI- and GRE-based susceptibility mapping.

[0144] Apart from this, the generally low variability of the susceptibility values across the multiple repetitions indicates a high stability of the technique. As displayed in Figures 11A to 11C, higher variabilities across repetitions were found to be a consequence of head motion introducing a misregistration between anatomy and brain mask used for QSM processing. The associated susceptibility drift mostly affects smaller and more inferior brain regions such as the pallidum. While this drift is considered reversible by adjusting the brain mask for every single volume, the significant amount of blurring observed for the time averaged with respect to the single-volume reconstruction underlines the importance of keeping the acquisition time short and highlights the advantage of the proposed POP EPI acquisition over a standard GRE scheme.

[0145] Whilst a regular azimuthal distribution of the trajectories was used, it will be appreciated that the proposed readout schemes provide a high adaptability, and the most suitable sampling and reconstruction technique can be chosen according to the desired application. For example, a golden angle azimuthal order, as well as sliding window or filtered reconstruction techniques for example may be used to enhance the spatio-temporal flexibility in applications like functional MRI. POP readout schemes are also considered to support higher undersampling factors than comparable Cartesian acquisition schemes. Another major benefit of the radial character of the 3D POP EPI readout scheme is its robustness to motion. Also sampling the center of k-space with each trajectory opens up opportunities for advanced phase and motion corrections, which can be particularly helpful when scanning patient populations. The slight contrast increase that was found for 3D POP EPI with respect to 3D GRE tends to be more obvious for the protocols with longer repetition time, and is most likely the result of the longer readout in the EPI protocols.

[0146] Optimizations of the sequence timing and accurate third order shimming can be beneficial, as is the use of a gradient delay or Nyquist ghost correction. Besides correcting for echo shifts within each individual readout trajectory, this also helps align the central readout points of all trajectories on top of each other.

[0147] In the specific example, phase correction was based on additional navigator lines that were acquired for every trajectory prior to the actual echo-planar readout. To improve the fit stability for the gradient delay estimation, an azimuthal distribution of the trajectories over 2π rather than π was chosen. The phase correction successfully removed Nyquist ghosting and increased the signal homogeneity across the brain. It also had a major positive effect on the image reconstruction. Skipping the phase correction leads to discontinuities in *k*-space when combining the segmentation or GRAPPA calibration subsets, introducing residual artefacts either directly or through miscalibration of the GRAPPA kernel. Minor other effects that are considered to be a result of improving the trajectory alignment were a slight reduction in background noise and some slight removal of blurring artefacts. However, these effects appeared to be rather small.

[0148] If more severe gradient delays or major eddy current induced trajectory errors are present, prospective correction techniques, a gradient field camera, or designated data driven methods may be employed to improve results. For simplicity, ramp sampling regridding was performed before the phase correction, which can introduce edge ghosting. While no significant effects were observed in this work, incorporating the ramp sampling regridding step into the non-uniform fast Fourier transform could enhance the reconstruction quality.

[0149] Further improvements in image quality can also be obtained using field map approaches or non-linear image registration algorithms, which provide a means to overcome geometric distortions.

[0150] QSM processing was performed for every single channel in this study, which in contrast to coil-combined approaches can be considered computationally expensive. However, using parallel computing on a dedicated computing cluster, the processing time could be kept within a reasonable range. Employing POP-type readout schemes usually

involves rotating the phase encoding direction with respect to standard 3D GRE and comparable Cartesian readout schemes. As a consequence, the minimum echo time is limited by the matrix size in the head–foot (usually the partition direction in conventional 3D imaging) rather than in the anterior–posterior (usually the phase encoding direction in conventional 3D imaging) direction. In high resolution whole brain applications this provides a significant benefit to minimize echo time, since the matrix size along the head–foot direction is usually smaller due to the geometry of the brain.

[0151] In this study, three-shot segmentation or parallel imaging with an undersampling factor of $R_{PE} = 3$ was applied along the phase encoding direction. Thus, whole brain coverage at echo times of $T_E = 12$ ms, 16 ms and 21 ms could be achieved by making use of partial Fourier undersampling factors of PF = 5/8, 6/8 and 7/8, respectively. The associated zero-filling in the reconstruction generally did not affect the image quality. However, for the protocol with the highest partial Fourier undersampling ($T_E = 12$ ms) signal dropouts in the inferior brain regions slightly increased. Here improvements may be achieved using phase constrained reconstruction approaches. For the accelerated protocol, images could be reconstructed without significant residual artefacts.

[0152] Apart from the decreased SNR, higher order effects of non-linear phase differences appeared loosely near areas of high susceptibility gradients. These effects, which are particularly known for high resolution ultra-high field EPI, can be corrected for by employing a sophisticated parallel imaging reconstruction. Major noise enhancement has not been observed. For reasons of simplicity a TGRAPPA like interleaved acquisition scheme was chosen, which allowed extraction of the calibration data from the scan data itself. Thus, additional calibration scans were not required and artefacts related to different levels of distortion in calibration and scan data could be avoided.

[0153] Regarding the susceptibility mapping results, no substantial differences are found when comparing the different ultra-high field 3D POP EPI protocols used in this study. Considering the image quality and taking into account the time required for scan and calibration, using the accelerated protocol is potentially most beneficial in cases where subject motion is highly likely. Apart from this, employing PF = 6/8 is considered to provide

the best trade-off between echo-time minimization on the one hand and image quality on the other.

[0154] At lower field strengths such as 1.5 T or 3 T, where longer echo times are usually acceptable and adverse effects such as distortions are less pronounced, partial Fourier undersampling may not be necessary, meaning the proposed readout scheme should also be well suited for these field strength.

[0155] Accordingly, the above examples demonstrate that high resolution accelerated QSM can be performed using non-Cartesian 3D POP EPI at ultra-high field. The proposed technique is considerably faster than the conventional Cartesian 3D multi-echo GRE approach, while yielding comparable susceptibility values in subcortical structures. The proposed non-Cartesian POP readout scheme allows for an echo time suitable for susceptibility mapping, reduced echo train lengths and reduced distortions with respect to conventional Cartesian EPI. Providing high flexibility in terms of undersampling renders POP EPI also interesting for other applications such as functional MRI.

[0156] In another further study, an asymmetric readout scheme is created as shown in Figures 4D and 4E. Shifting the echo directly translates into higher spatial frequencies sampled during the acquisition. This creates undersampled areas in *k*-space, but does not change the acquisition time and has minimal impact on TE.

[0157] The concept was evaluated in a healthy volunteer using a 7 T whole-body research MRI scanner (Siemens Healthcare, Erlangen, Germany) under Institutional review board permission. The system was equipped with a Tx/32 channel Rx head array (Nova Medical, USA). Third order shimming was employed for all measurements.

[0158] 3D POP EPI Images were obtained at 1 mm isotropic spatial resolution using following acquisition parameters: FOV = 212 x 212 x 108mm^3, 360 projections, T_R = 47 ms, T_E = 24 ms, ES= 1.0 ms, flip angle= 13°, ramp sampling= 20%, 3-fold segmentation along phase encoding direction, acquisition time = 51 seconds. At the beginning of each readout train, 3 additional navigator echoes were acquired and an interleaved radial projection order was used to achieve a homogeneous azimuthal distribution of the trajectories as shown in

Figure 4E. Additional scans with the same parameters and echo asymmetries of 9%, 19% and 28% were performed to achieve spatial resolutions of 0.9 x 0.9 x 1.0 mm^3, 0.84 x 0.84 x 1.0 mm^3, 0.78 x 0.78 x 1.0 mm^3. In this instance, the use of a POP with asymmetric readout train (POP-ART) readout scheme entails undersampling of the higher spatial frequencies in *k*-space with undersampling factors of 2.0, 2.2 and 2.4.

[0159] Image reconstruction was performed offline using MATLAB (MathWorks, Natick, MA, USA). After combination of the segmentation subsets and phase correction, the individual readout trajectories were Fourier transformed along the phase encoding axis and gridded onto a Cartesian grid using the non-uniform fast Fourier transform (NUFFT) software. The ramp sampling interpolation was incorporated in the final gridding step.

[0160] Representative results are shown in Figures 12A and 12B. The improvement in spatial resolution with increasing echo asymmetry is clearly visible. The different POP-ART acquisitions provide similar image quality and, as expected, show similar behaviour in terms geometric distortions and signal dropouts. Some reconstruction artefacts are observed as low level high frequency streaking, as expected from the slight radial undersampling.

[0161] The clear resolution improvement is demonstrated in greater detail in Figure 13, which depicts two enlarged sections of the brain and compares the results between the conventional 3D POP scan and the asymmetric 3D POP-ART acquisition with 28% echo asymmetry.

[0162] High resolution 3D POP-ART EPI imaging was successfully performed at ultra-high field. Without echo-time or acquisition time adjustments, an almost 2-fold improvement in spatial resolution was achieved with respect to conventional 3D POP EPI by using an echo-asymmetry of only 28%. The trajectory facilitates spatial resolutions that cannot be achieved with a corresponding Cartesian 3D EPI protocol. With acquisition times on the order of 1 minute, the proposed approach is considerably faster than a corresponding standard Cartesian 3D GRE protocol.

[0163] The radial nature of the POP-ART readout scheme is beneficial in terms of motion robustness and provides high flexibility for undersampling. The concept is of interest for high resolution for T_2* weighted imaging or quantitative susceptibility mapping of the brain.

[0164] Throughout this specification and claims which follow, unless the context requires otherwise, the word “comprise”, and variations such as “comprises” or “comprising”, will be understood to imply the inclusion of a stated integer or group of integers or steps but not the exclusion of any other integer or group of integers. As used herein and unless otherwise stated, the term "approximately" means ±20%.

[0165] Persons skilled in the art will appreciate that numerous variations and modifications will become apparent. All such variations and modifications which become apparent to persons skilled in the art, should be considered to fall within the spirit and scope that the invention broadly appearing before described.

THE CLAIMS DEFINING THE INVENTION ARE AS FOLLOWS:

1) A magnetic resonance imaging method for imaging an anatomical region of a subject, the method comprising:
   a) generating an imaging field, the anatomical region being provided in an acquisition space within the imaging field;
   b) generating multiple acquisition sequences, each acquisition sequence including an RF excitation pulse, and gradient field pulses configured to generate a readout trajectory in *k*-space, each readout trajectory including a number of scan lines extending in a frequency encoding direction and spaced in a second phase encoding direction along a phase encoding axis, and the multiple acquisition sequences generating a plurality of readout trajectories extending over at least part of an acquisition space, the readout trajectories being rotated at least partially about the phase encoding axis;
   c) acquiring echo signals from the readout trajectories for each of the multiple acquisition sequences to generate *k*-space data; and,
   d) processing the *k*-space data to generate at least one image representation of the anatomical region.
2) A method according to claim 1, wherein the method includes undersampling in at least one of a radial and a phase encoding direction.
3) A method according to claim 2, wherein the readout trajectories are undersampled with an undersampling factor of $R_{PE} > 1$ to shorten echo signal acquisition times.
4) A method according to claim 2 or claim 3, wherein the method includes undersampling to acquire echo signals from selected scan lines of a trajectory, thereby missing at least some scan lines.
5) A method according to claim 4, wherein the method includes acquiring echo signals from missing scan lines in subsequent acquisitions.
6) A method according to claim 5, wherein the method includes acquiring echo signals from at least one of:
   a) interleaved scan lines of multiple trajectories; and,
   b) block-wise segmented trajectories.
7) A method according to claim 4, wherein the method includes performing accelerated imaging by reconstructing data from missing scan lines.

8) A method according to claim 6, wherein the method includes reconstructing data using at least one of:
   a) echo signals acquired from different scan lines in the trajectory;
   b) echo signals acquired from scan lines of different trajectories;
   c) echo signals acquired from scan lines of adjacent trajectories;
   d) echo signals acquired from equivalent different scan lines of adjacent trajectories and,
   e) echo signals acquired from different scan lines of adjacent trajectories.
9) A method according to any one of the claims 1 to 8, wherein the method includes sampling at least one common scan line in two different readout trajectories with different echo times.
10) A method according to any one of the claims 1 to 9, wherein the multiple readout trajectories are asymmetrically arranged with respect to the phase encoding axis.
11) A method according to claim 10, wherein the degree of asymmetry changes during acquisition.
12) A method according to any one of the claims 1 to 11, wherein the method includes applying multiple acquisition sequences to generate a homogeneous azimuthal distribution of readout trajectories.
13) A method according to any one of the claims 1 to 12, wherein the readout trajectories are distributed by an azimuthal angle Θ given by:

$$\Theta_j = \frac{(j-1)2\pi}{N} + \vartheta(j)$$

where: N denotes the number of trajectories

$$\vartheta(j) = \begin{cases} 0 & f \quad 1 \le j \le N/2 \\ \pi/N[(N-1)m \quad 2]\, f & N/2 < j \le N \end{cases}$$

14) A method according to any one of the claims 1 to 13, wherein the method includes generating readout trajectories spaced by a golden angle.
15) A method according to any one of the claims 1 to 14, wherein the method includes generating readout trajectories spaced by an azimuthal angle given by:

$$\Delta\Theta = {}^{\pi}/_{(1+\sqrt{5})/2 + Q - 1}$$

where Q can be any integer number.

16) A method according to any one of the claims 1 to 15, wherein the method includes generating readout trajectories spaced by a random azimuthal angle increment.

17) A method according to any one of the claims 1 to 16, wherein the readout trajectory is rotated about the phase encoding axis as the phase encoded signals are acquired to define a curved readout trajectory.

18) A method according to any one of the claims 1 to 17, wherein the phase encoding axis is orientated at least one of:

a) along a shortest dimension of the anatomical region;

b) perpendicular to a trajectory of the at least one image representation; and,

c) perpendicular to a transverse trajectory of the subject.

19) A method according to any one of the claims 1 to 18, wherein a variation of the azimuthal angle of the readout trajectory is defined by a variation of the amplitude of pulses in readout gradient fields.

20) A method according to any one of the claims 1 to 19, wherein an asymmetry about a phase encoding axis is controlled based on an amplitude of dephaser pulses in readout gradient fields.

21) A method according to any one of the claims 1 to 20, wherein at least one acquisition sequence includes at least one of:

a) an RF excitation pulse; and,

b) a preparation module include one or more pulses.

22) A method according to any one of the claims 1 to 21, wherein the method of reconstructing data includes at least one of:

a) performing phase correction;

b) at least one of:

i) combining echo signals from multiple trajectories; and,

ii) reconstructing missing data from undersampled trajectories;

c) performing a Fourier transform along a phase encoding axis;

d) regridding to a uniform grid; and,

e) combining individual data subsets into a combined dataset.

23) A method according to any one of the claims 1 to 22, wherein the method of reconstructing data exploits the symmetry of *k*-space.

24) A method according to any one of the claims 1 to 23, wherein the method of acquisition and reconstructing data uses partial Fourier techniques.

25) A method according to any one of the claims 1 to 24, wherein the method of reconstructing includes filtering of *k*-space data.

26) A method according to any one of the claims 1 to 25, wherein the method of reconstructing uses at least one of:

a) prior knowledge;

b) prior knowledge of different echo-times of individual trajectories;

c) prior knowledge of contrasts of individual trajectories; and,

d) a model-based reconstruction.

27) A method according to any one of the claims 1 to 26, wherein the method includes processing the *k*-space data by interpolating echo signals onto equidistant sampling points along a readout axis to remove non-linearities.

28) A method according to any one of the claims 1 to 27, wherein the method includes processing the *k*-space data by performing, for echo signals of at least one readout trajectory, at least one of:

a) gradient delay;

b) Nyquist ghost correction;

c) physiologic noise correction; and,

d) eddy current corrections.

29) A method according to any one of the claims 1 to 28, wherein the method includes processing the *k*-space data by:

a) acquiring one or more non-phase-encoded navigator echo signals between each RF excitation and acquiring echo signals from the readout trajectories;

b) estimating a gradient delay induced shift along a readout axis; and,

c) correcting for gradient delays using the estimated gradient delay.

30) A method according to any one of the claims 1 to 29, wherein the method includes processing the *k*-space data by:

a) obtaining shifts at multiple azimuthal readout trajectory angles;

b) fitting shift values to a gradient delay model; and,

c) using delay model fit values to correct for the linear phase errors between the odd and even scan lines.

31) A method according to any one of the claims 1 to 30, wherein the method includes processing the *k*-space data for at least one of:

a) susceptibility mapping; and,

b) relaxation time mapping.

32) A magnetic resonance imaging apparatus for imaging an anatomical region of a subject, the apparatus comprising:

a) a magnetic resonance imaging device; and,

b) one or more processing devices that:

i) control the magnetic resonance imaging device to cause the magnetic resonance imaging device to:

(1) generate an imaging field, the anatomical region being provided in an acquisition space in the imaging field;

(2) generate multiple acquisition sequences, each acquisition sequence including an RF excitation pulse, and gradient field pulses configured to generate a readout trajectory in *k*-space, each readout trajectory including a number of scan lines extending in a frequency encoding direction and spaced in a second phase encoding direction along a phase encoding axis, and the multiple acquisition sequences generating a plurality of readout trajectories extending over at least part of the acquisition space, the readout trajectories being rotated at least partially about the phase encoding axis;

(3) acquire echo signals from the readout trajectories for each of the multiple acquisition sequences to generate *k*-space data; and,

ii) process the *k*-space data to generate at least one image representation of the anatomical region.

33) A magnetic resonance imaging method for imaging an anatomical region of a subject, the method comprising:

a) generating an imaging field, the anatomical region being provided in an acquisition space in the imaging field;

b) generating multiple acquisition sequences, each acquisition sequence including an RF excitation pulse, and gradient field pulses configured to generate a readout trajectory in *k*-space, each readout trajectory including a number of scan lines extending in a frequency encoding direction and spaced in a second phase encoding direction along a phase encoding axis, and the multiple acquisition sequences generating a plurality of readout trajectories extending over at least part of the acquisition space, wherein at least one acquisition sequence is undersampled in at least one of a frequency and a phase encoding direction;

c) acquiring echo signals from the multiple readout sub-trajectories for each of the multiple acquisition sequences to generate *k*-space data including reconstructed readout trajectories; and,

d) processing the *k*-space data to generate at least one image representation of the anatomical region.

34) A method according to claim 33, wherein the method includes undersampling in at least one of a radial and a phase encoding direction.

35) A method according to claim 34, wherein the readout trajectories are undersampled with an undersampling factor of $R_{PE} > 1$ to shorten echo signal acquisition times.

36) A method according to claim 34 or claim 35, wherein the method includes undersampling to acquire echo signals from selected scan lines of a trajectory, thereby missing at least some scan lines.

37) A method according to claim 36, wherein the method includes acquiring echo signals from missing scan lines in subsequent acquisitions.

38) A method according to claim 37, wherein the method includes acquiring echo signals from at least one of:

a) interleaved scan lines of multiple trajectories; and,

b) block-wise segmented trajectories.

39) A method according to claim 36, wherein the method includes performing accelerated imaging by reconstructing data from missing scan lines.

40) A method according to claim 39, wherein the method includes reconstructing data using at least one of:

a) echo signals acquired from different scan lines in the trajectory;

b) echo signals acquired from scan lines of different trajectories;

c) echo signals acquired from scan lines of adjacent trajectories;

d) echo signals acquired from equivalent different scan lines of adjacent trajectories and,

e) echo signals acquired from different scan lines of adjacent trajectories.

41) A method according to any one of the claims 33 to 40, wherein the method includes sampling at least one common scan line in two different readout trajectories with different echo times.

42) A method according to any one of the claims 33 to 41, wherein the phase encoding axis is orientated at least one of:

a) along a shortest dimension of the anatomical region;

b) perpendicular to a trajectory of the at least one image representation; and,

c) perpendicular to a transverse trajectory of the subject.

43) A method according to any one of the claims 33 to 42, wherein the method of reconstructing data includes at least one of:

a) performing phase correction;

b) at least one of:

i) combining echo signals from multiple trajectories; and,

ii) reconstructing missing data from undersampled trajectories;

c) performing a Fourier transform along a phase encoding axis;

d) regridding to a uniform grid; and,

e) combining individual data subsets into a combined dataset.

44) A method according to any one of the claims 33 to 43, wherein the method of reconstructing data exploits the symmetry of *k*-space.

45) A method according to any one of the claims 33 to 44, wherein the method of acquisition and reconstructing data uses partial Fourier techniques.

46) A method according to any one of the claims 33 to 45, wherein the method of reconstructing includes filtering of *k*-space data.

47) A method according to any one of the claims 33 to 46, wherein the method of reconstructing uses at least one of:

a) prior knowledge;

b) prior knowledge of different echo-times of individual trajectories;

c) prior knowledge of contrasts of individual trajectories; and,

d) a model-based reconstruction.

48) A method according to any one of the claims 33 to 47, wherein the method includes processing the *k*-space data by interpolating echo signals onto equidistant sampling points along a readout axis to remove non-linearities.

49) A method according to any one of the claims 33 to 48, wherein the method includes processing the *k*-space data by performing, for echo signals of at least one readout trajectory, at least one of:

a) gradient delay;

b) Nyquist ghost correction;

c) physiologic noise correction; and,

d) eddy current corrections.

50) A method according to any one of the claims 33 to 49, wherein the method includes processing the *k*-space data by:

a) acquiring one or more non-phase-encoded navigator echo signals between each RF excitation and acquiring echo signals from the readout trajectories;

b) estimating a gradient delay induced shift along a readout axis; and,

c) correcting for gradient delays using the estimated gradient delay.

51) A method according to any one of the claims 33 to 50, wherein the method includes processing the *k*-space data by:

a) obtaining shifts at multiple azimuthal readout trajectory angles;

b) fitting shift values to a gradient delay model; and,

c) using delay model fit values to correct for the linear phase errors between the odd and even scan lines.

52) A method according to any one of the claims 33 to 51, wherein the method includes processing the *k*-space data for at least one of:

a) susceptibility mapping; and,

b) relaxation time mapping.

53) A magnetic resonance imaging apparatus for imaging an anatomical region of a subject, the apparatus comprising:

a) a magnetic resonance imaging device; and,

b) one or more processing devices that:

i) control the magnetic resonance imaging device to cause the magnetic resonance imaging device to:

(1) generate an imaging field, the anatomical region being provided in an acquisition space in the imaging field;

(2) generate multiple acquisition sequences, each acquisition sequence including an RF excitation pulse, and gradient field pulses configured to generate a readout trajectory in *k*-space, each readout trajectory including a number of scan lines extending in a frequency encoding direction and spaced in a second phase encoding direction along a phase encoding axis, and the multiple acquisition sequences generating a plurality of readout trajectories extending over at least part of the acquisition space, wherein at least one of the acquisition sequences is undersampled in at least one of a frequency and phase encoding direction;

(3) acquire echo signals from the multiple readout sub-trajectories for each of the multiple acquisition sequences to generate *k*-space data including reconstructed readout trajectories; and,

ii) process the *k*-space data to generate at least one image representation of the anatomical region.

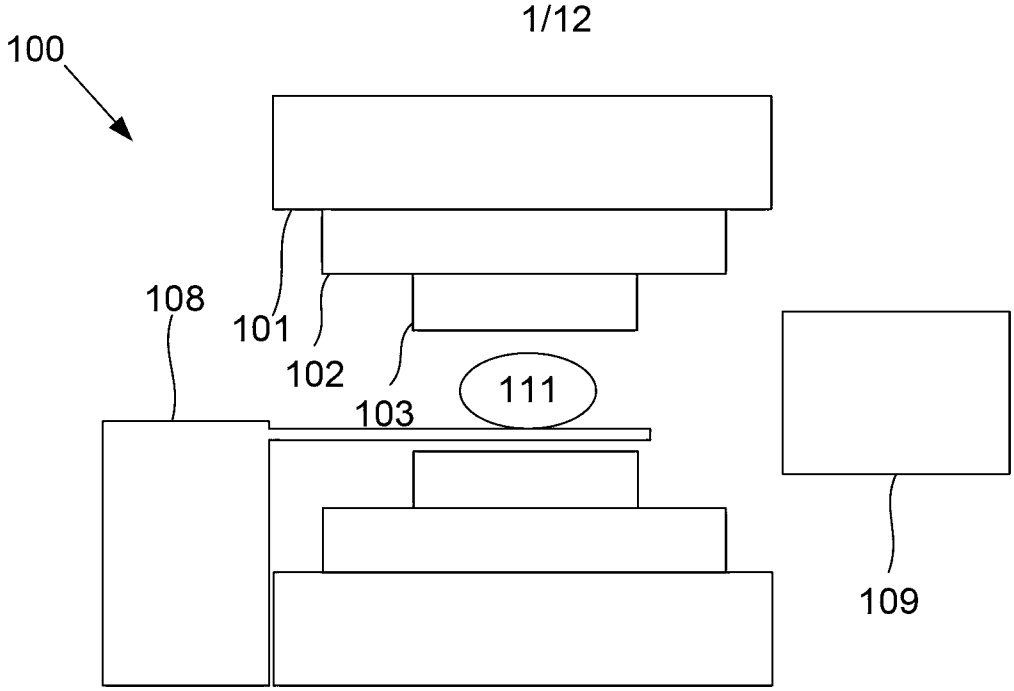


Fig. 1A

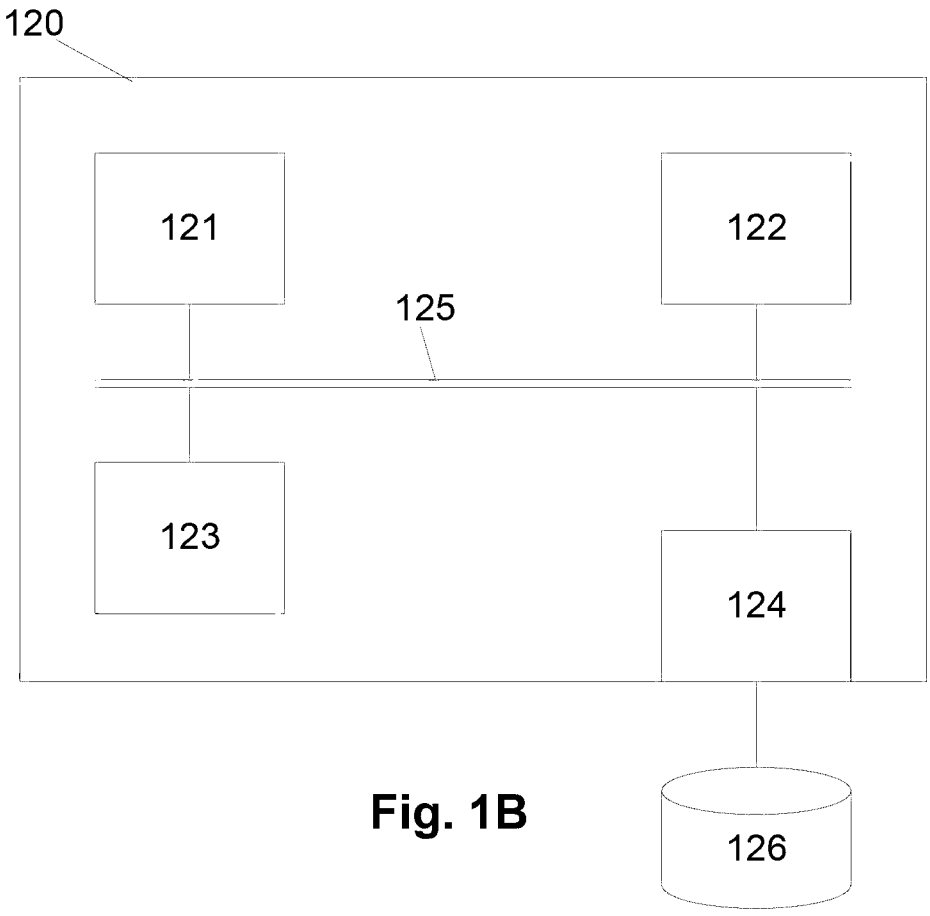


Fig. 1B

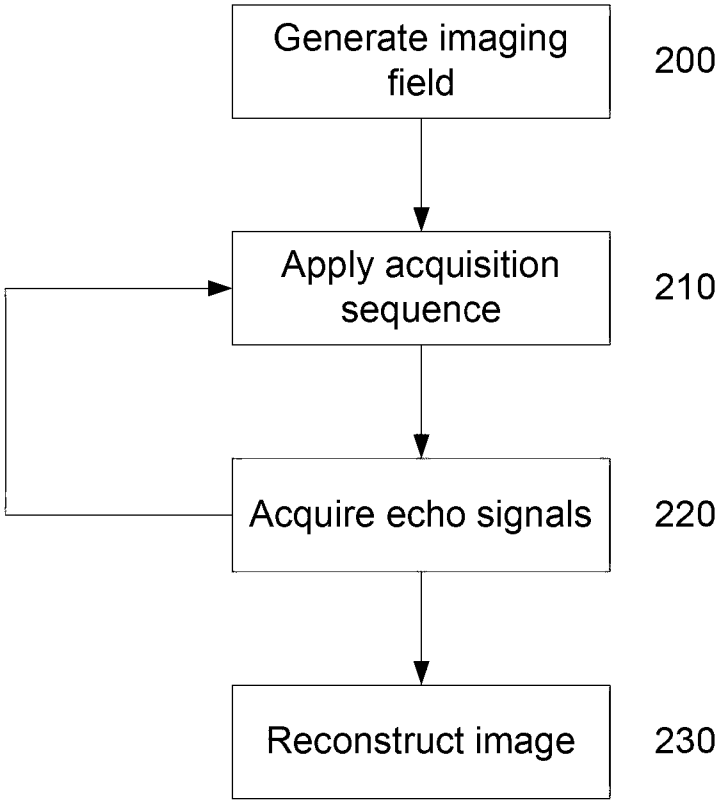

Generate imaging field
200
Apply acquisition sequence
210
Acquire echo signals
220
Reconstruct image
230

Fig. 2

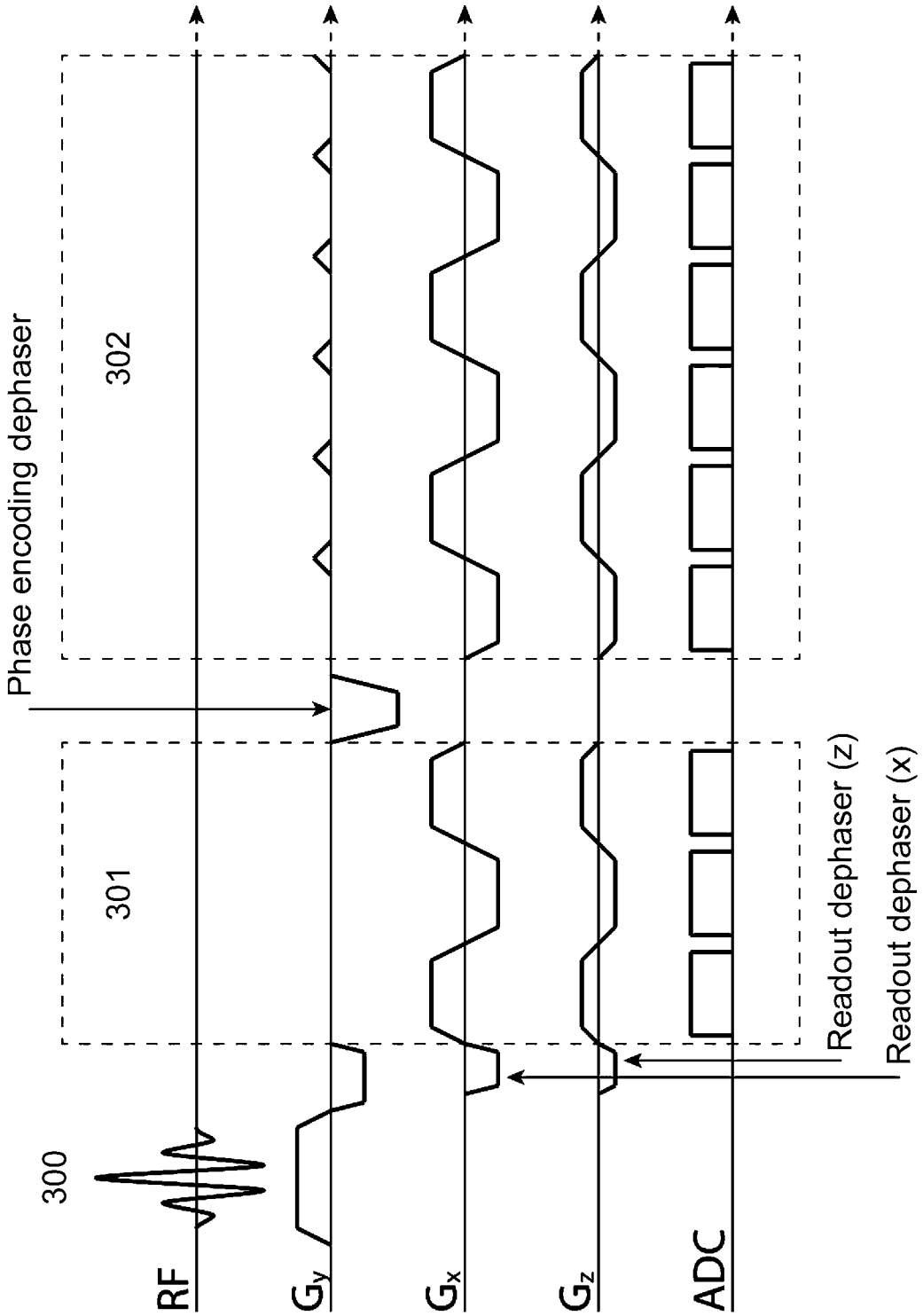
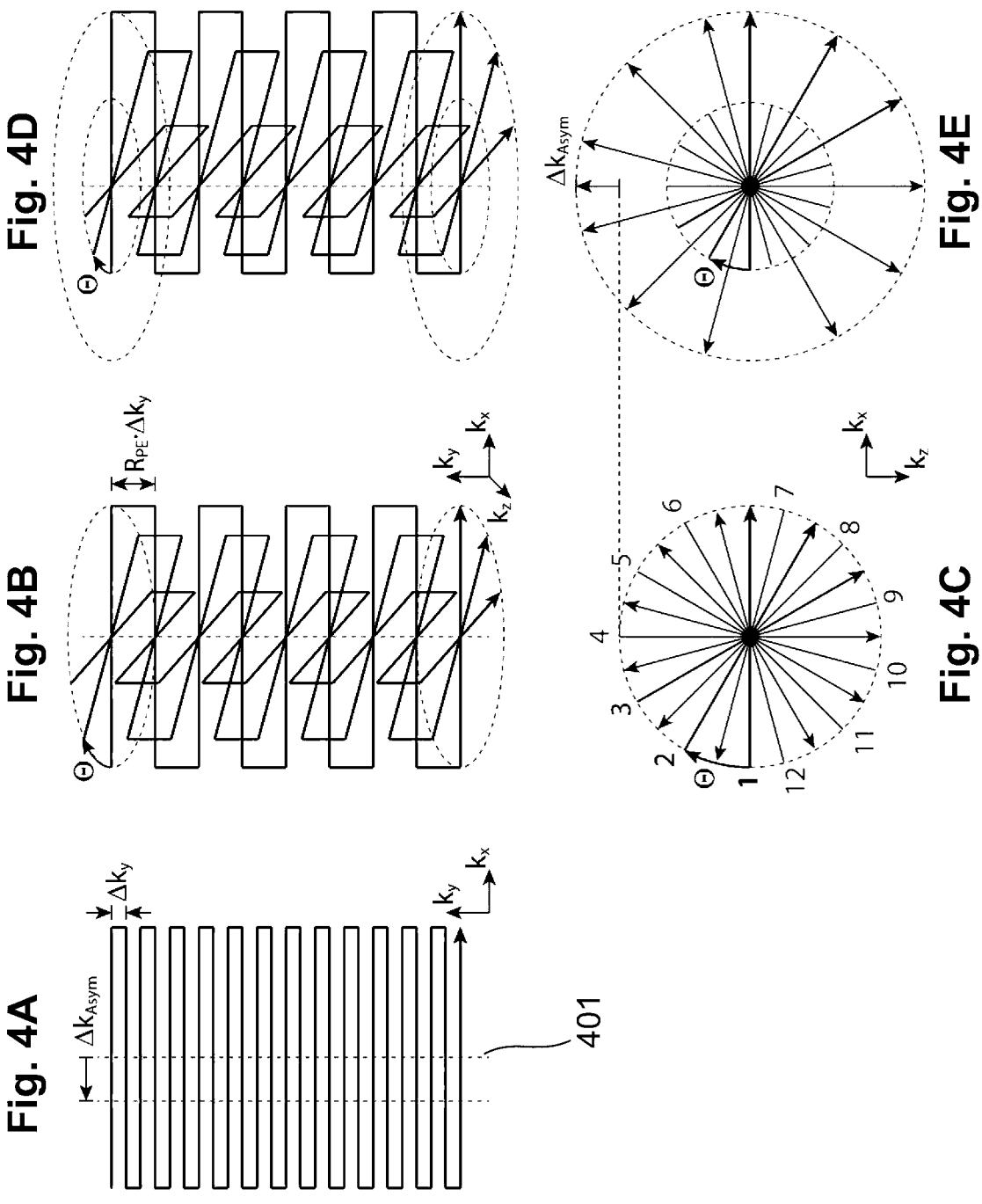

300
301
302
RF
G_y
G_x
G_z
ADC
Phase encoding dephaser
Readout dephaser (z)
Readout dephaser (x)

Fig. 3


Fig. 4A
Fig. 4B
Fig. 4C
Fig. 4D
Fig. 4E
401
Δk_{Asym}
Δk_y
$R_{PE} \cdot \Delta k_y$
k_x
k_y
k_z
1
2
3
4
5
6
7
8
9
10
11
12
Θ

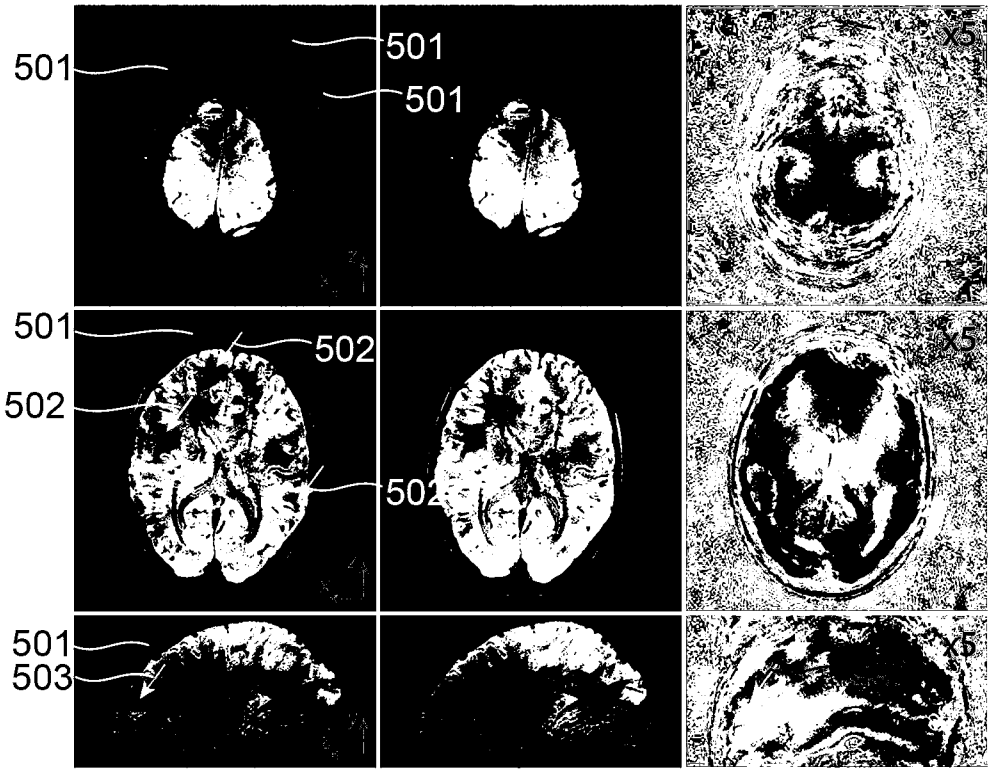

501
501
501
501
502
502
502
501
503
X5
X5
X5
X5

Fig. 5A

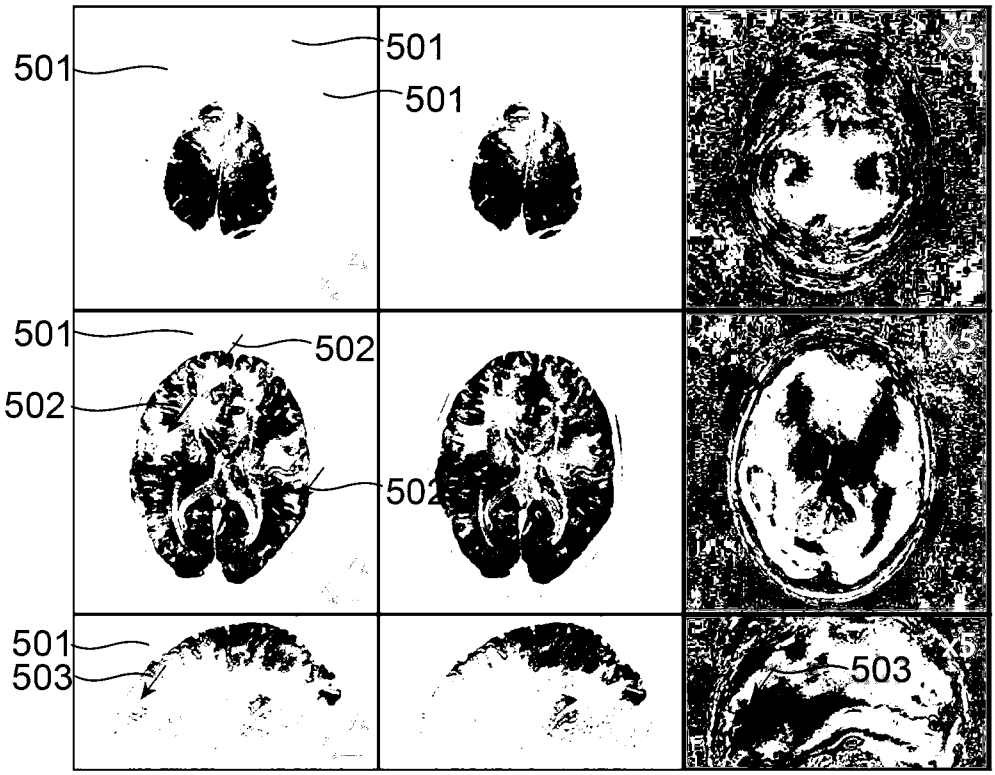

501
501
501
501
502
502
502
501
503
503
X5
X5
X5
X5

Fig. 5B

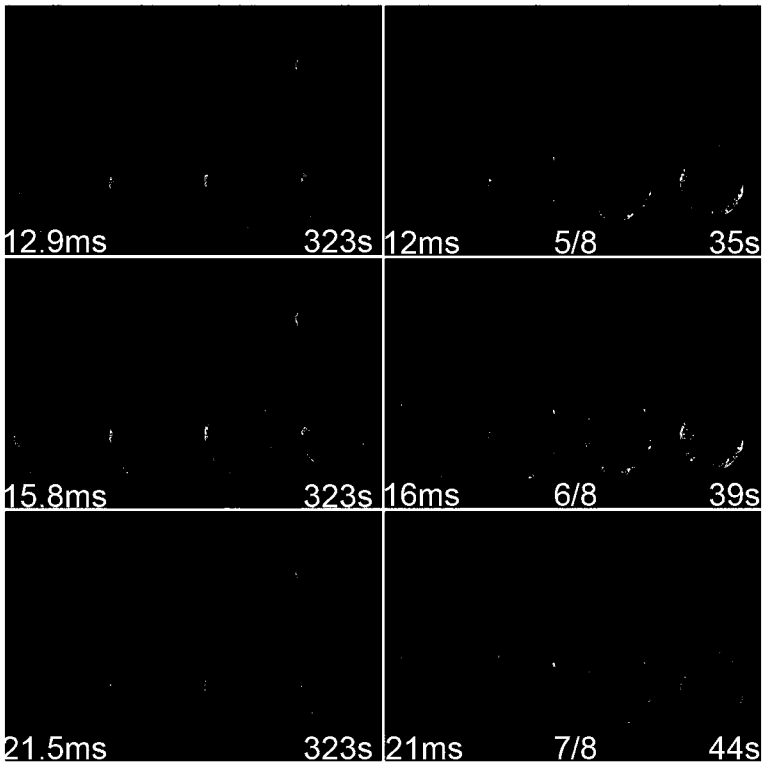

12.9ms 323s
12ms 5/8 35s
15.8ms 323s
16ms 6/8 39s
21.5ms 323s
21ms 7/8 44s

Fig. 6A

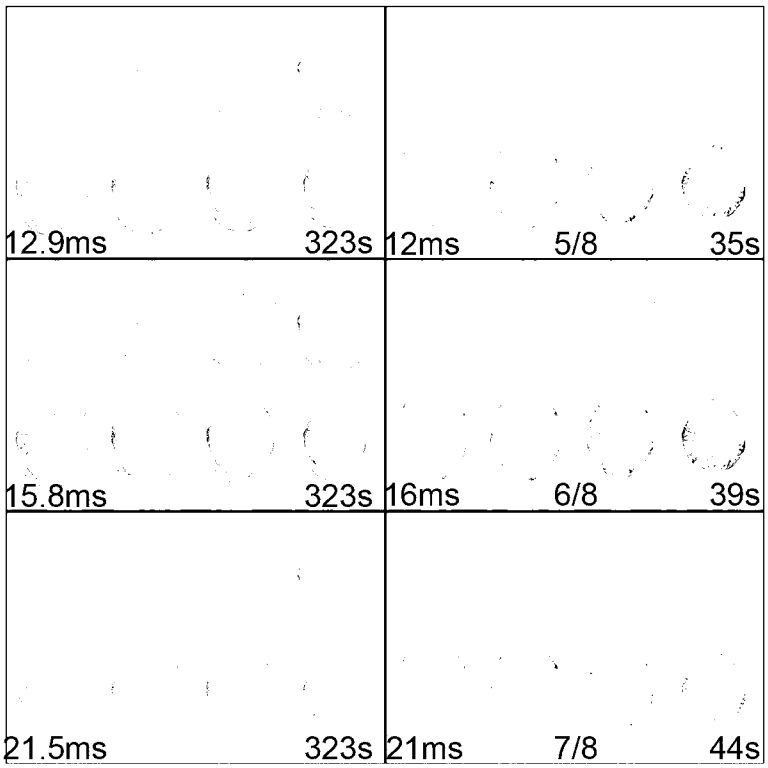

12.9ms 323s
12ms 5/8 35s
15.8ms 323s
16ms 6/8 39s
21.5ms 323s
21ms 7/8 44s

Fig. 6B

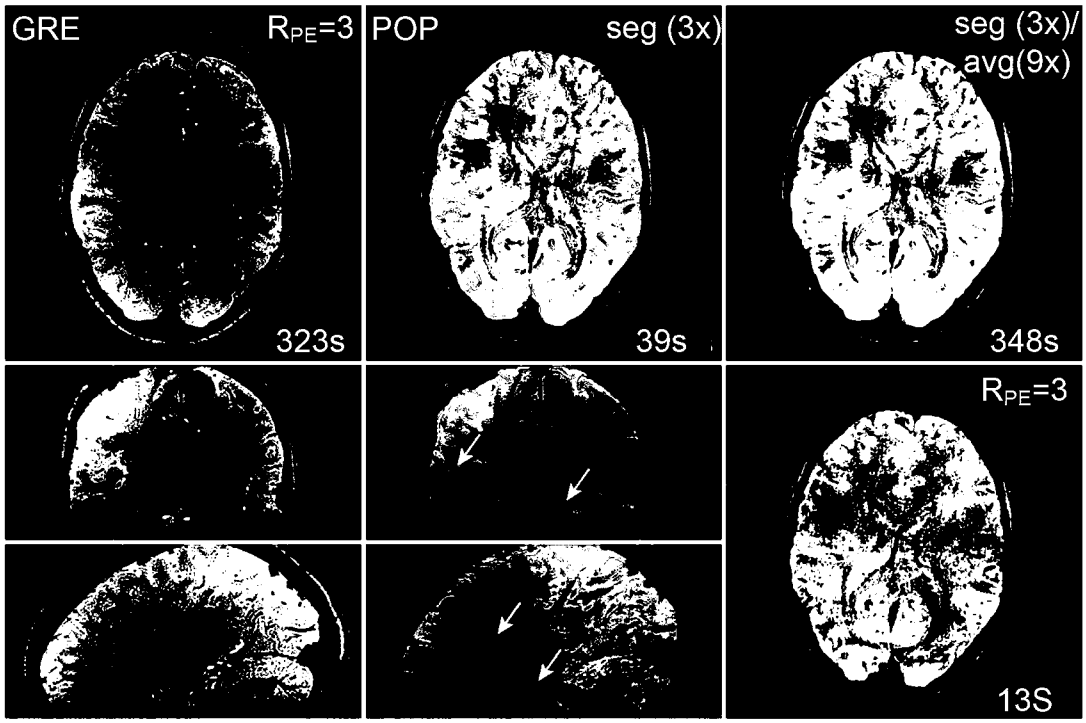

GRE
R_{PE}=3
323s
POP
seg (3x)
39s
seg (3x)/
avg(9x)
348s
R_{PE}=3
13S

Fig. 7A

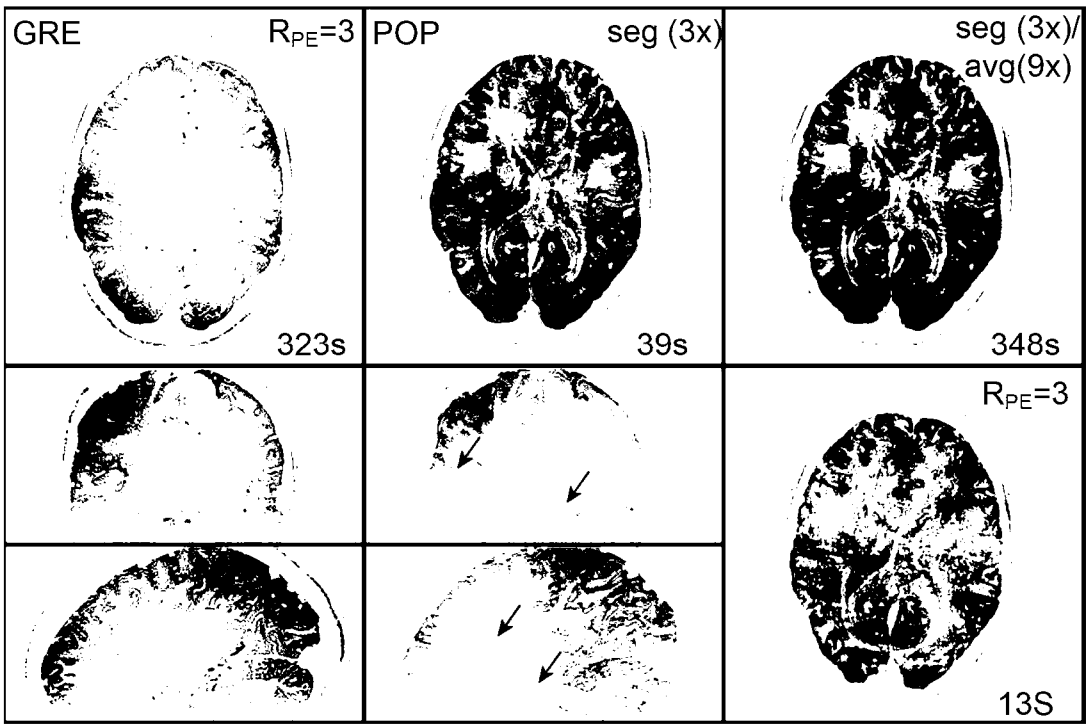

GRE
R_{PE}=3
323s
POP
seg (3x)
39s
seg (3x)/
avg(9x)
348s
R_{PE}=3
13S

Fig. 7B

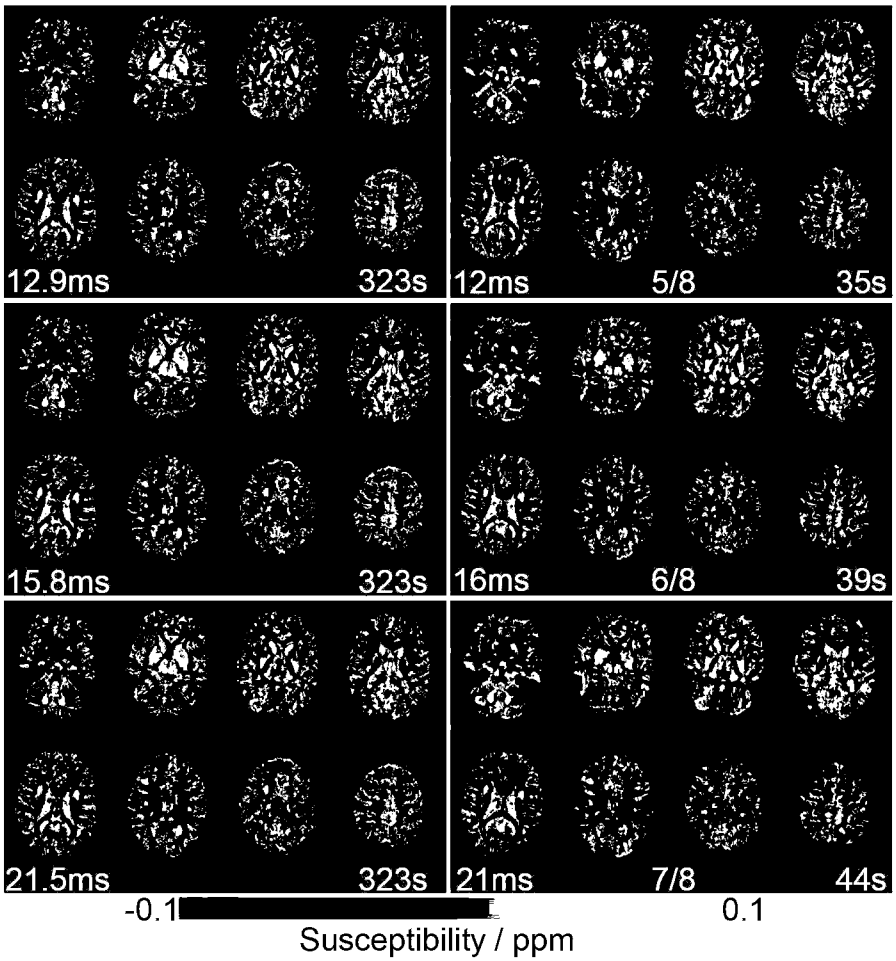

12.9ms
323s
12ms
5/8
35s
15.8ms
323s
16ms
6/8
39s
21.5ms
323s
21ms
7/8
44s
-0.1
0.1
Susceptibility / ppm

Fig. 8

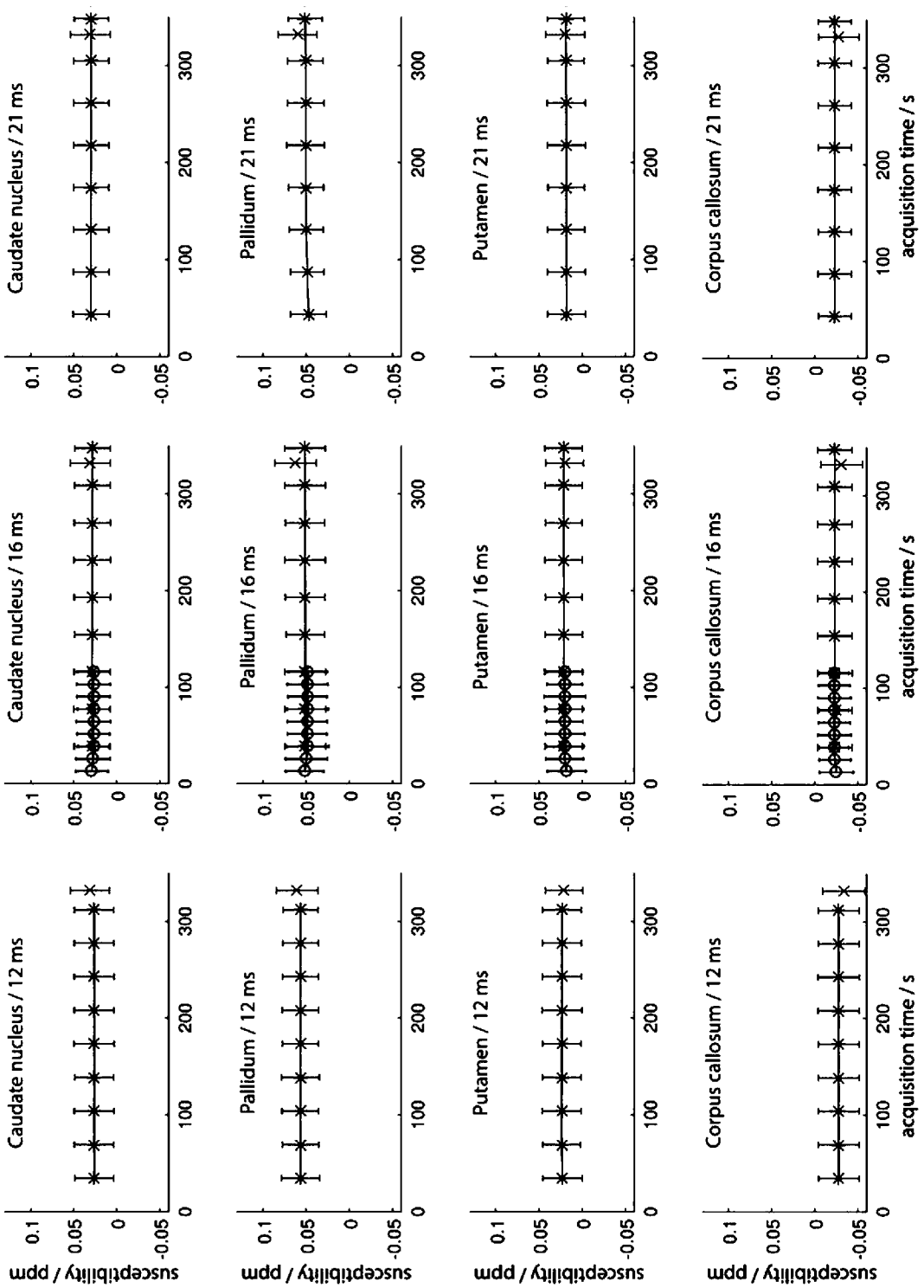

Caudate nucleus / 12 ms
Caudate nucleus / 16 ms
Caudate nucleus / 21 ms
Pallidum / 12 ms
Pallidum / 16 ms
Pallidum / 21 ms
Putamen / 12 ms
Putamen / 16 ms
Putamen / 21 ms
Corpus callosum / 12 ms
Corpus callosum / 16 ms
Corpus callosum / 21 ms
susceptibility / ppm
acquisition time / s
0.1
0.05
0
-0.05
0
100
200
300
* POP EPI seg. (3x)
O POP EPI (R = 3)
× GRE (R = 3)

Fig. 9

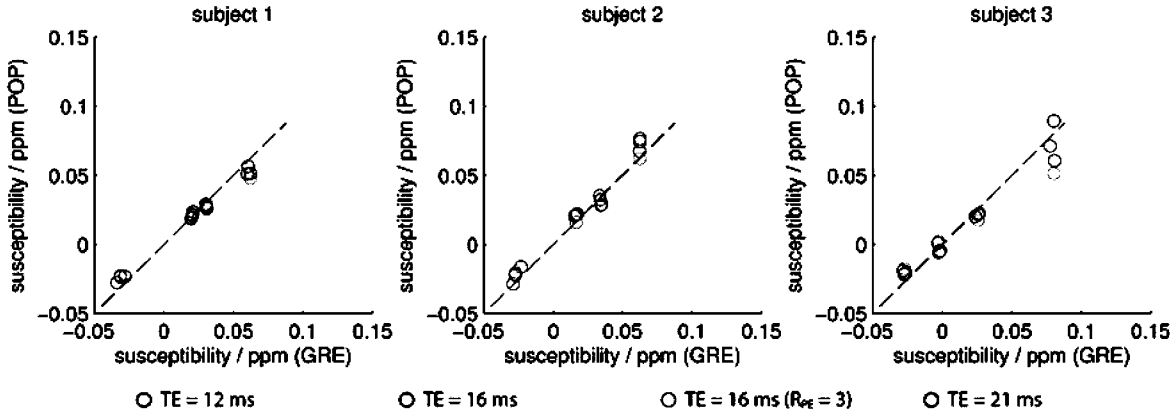


Fig. 10

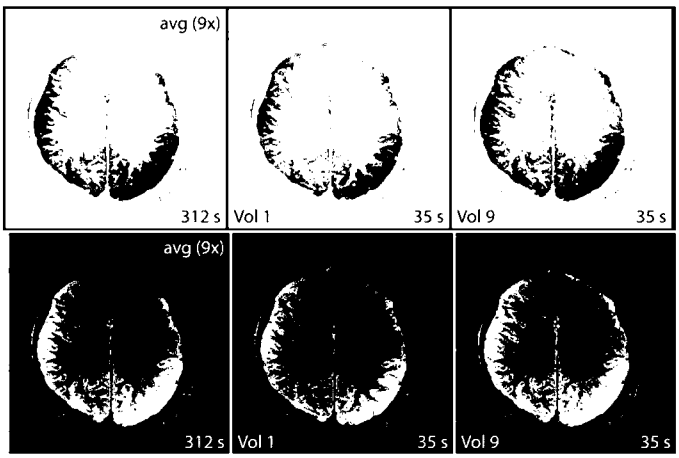


Fig. 11A

Fig. 11B

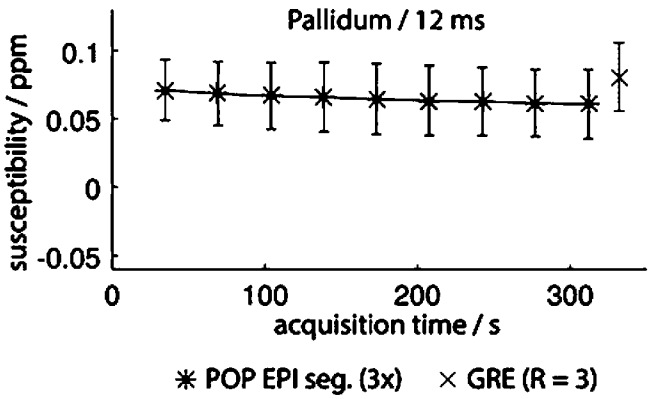


Fig. 11C

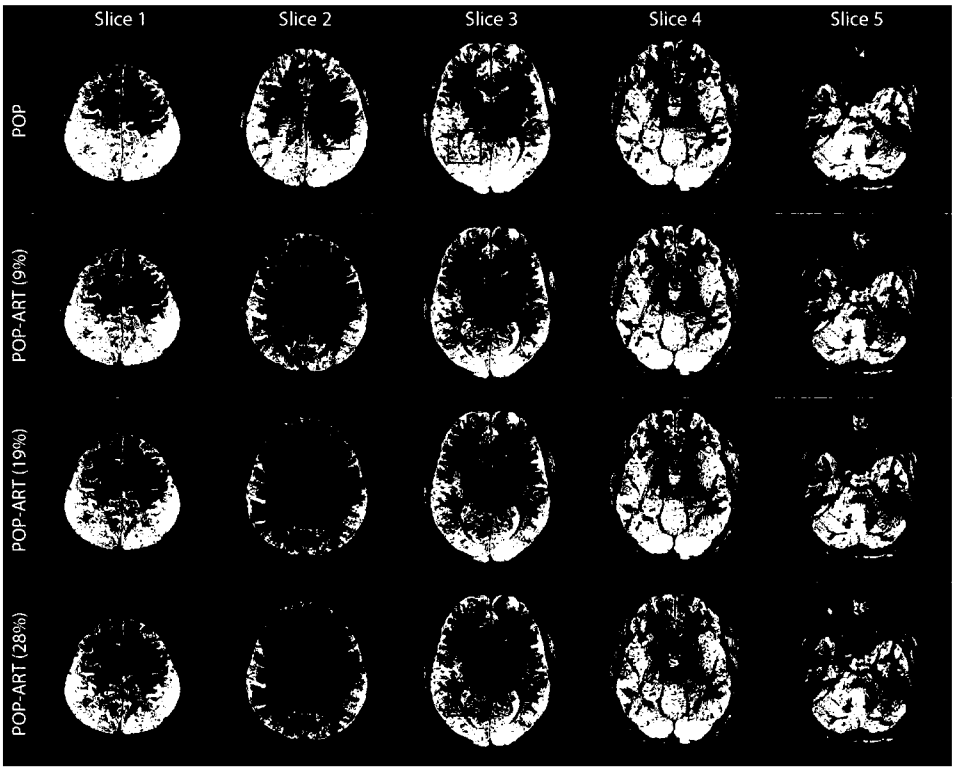


Fig. 12A

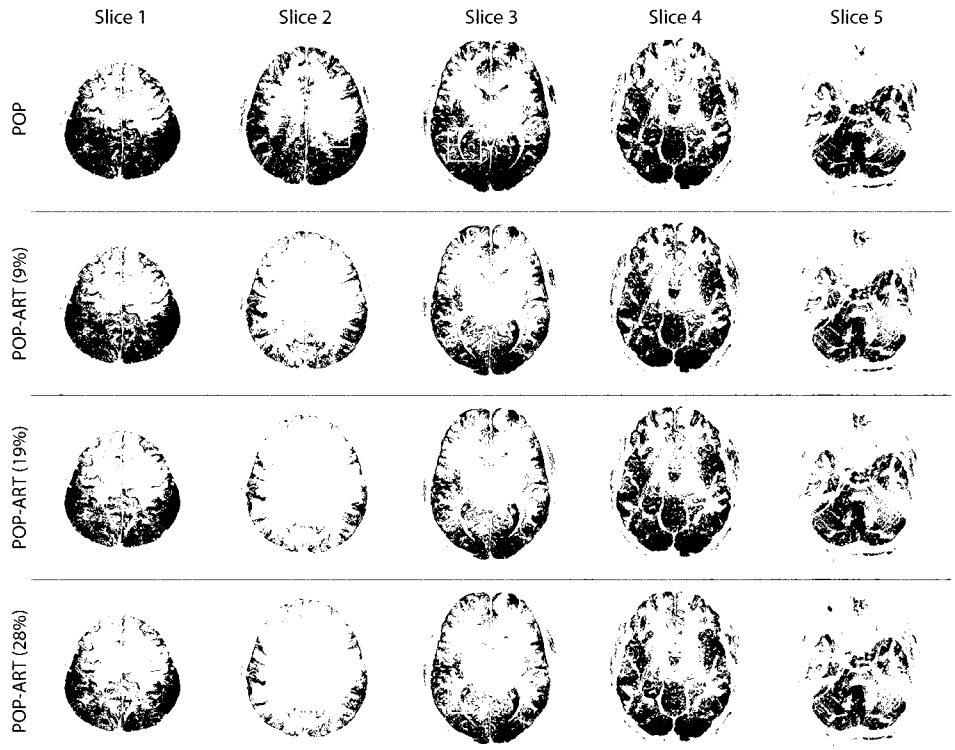


Fig. 12B

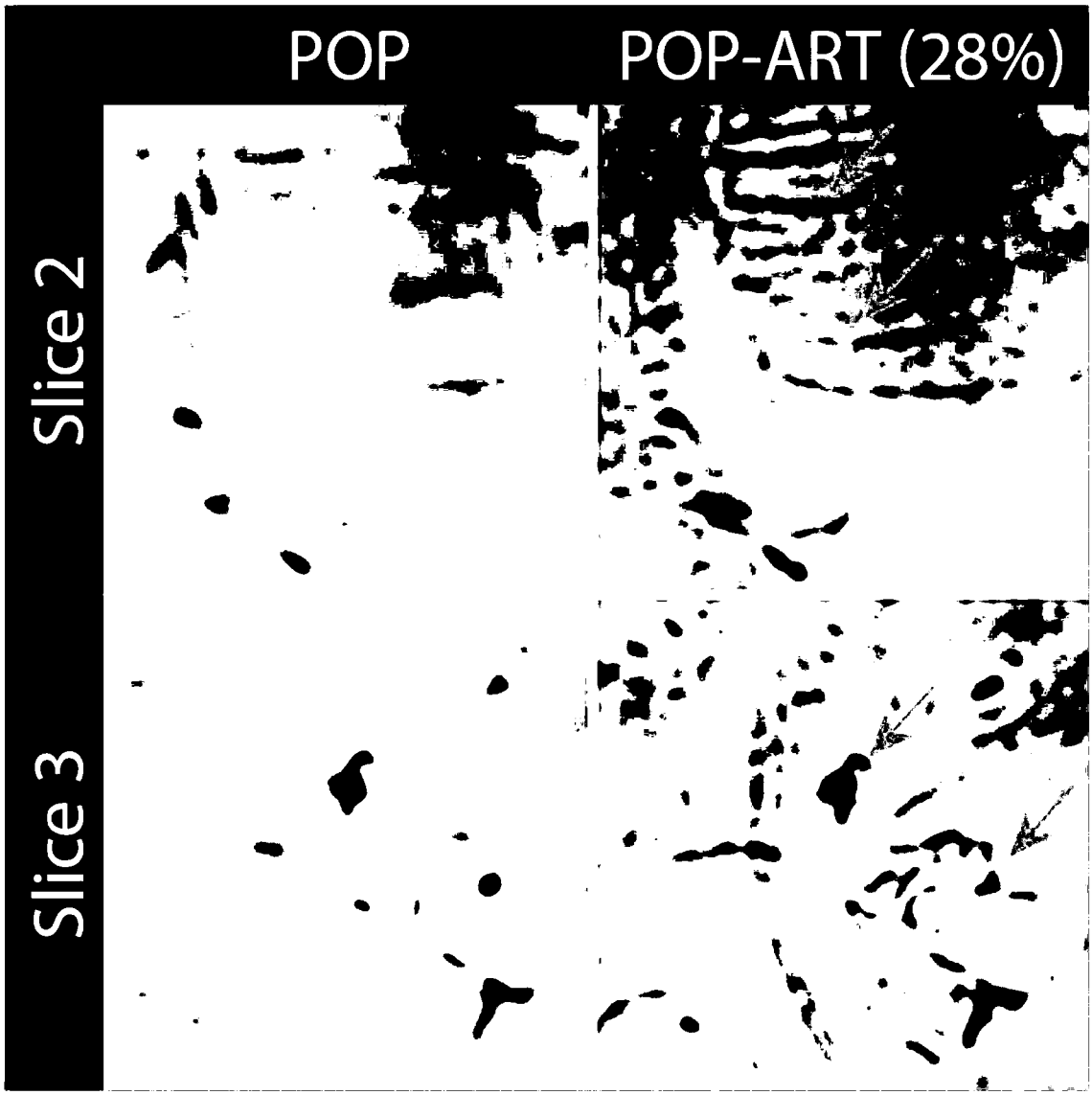


Fig. 13

INTERNATIONAL SEARCH REPORT

International application No.
PCT/AU2017/050294

A. CLASSIFICATION OF SUBJECT MATTER

G01R 33/20 (2006.01) A61B 5/055 (2006.01)

According to International Patent Classification (IPC) or to both national classification and IPC

B. FIELDS SEARCHED

Minimum documentation searched (classification system followed by classification symbols)

Documentation searched other than minimum documentation to the extent that such documents are included in the fields searched

Electronic data base consulted during the international search (name of data base and, where practicable, search terms used)

PATENTW, Espacenet, Google Patents, Google Scholar, Google

IPC: G01R 33/00; A61 5/055

CPC: G01R 33/243; G01R 33/246; G01R 33/4824; G01R 33/561

Keywords: magnet+, resona+, imag+, mri, QSM, quantita+, suscep+, k_space, phase encod+, freq+, encod+, rotat+, under_sampl+, trajec+, acquisition+ and similar terms

Applicant/Inventor name searched in Internal Databases provided by IP Australia, AUSPAT and Espacenet

C. DOCUMENTS CONSIDERED TO BE RELEVANT

Category*	Citation of document, with indication, where appropriate, of the relevant passages	Relevant to claim No.
	Documents are listed in the continuation of Box C	

[X] Further documents are listed in the continuation of Box C [X] See patent family annex

* Special categories of cited documents:

"A" document defining the general state of the art which is not considered to be of particular relevance

"E" earlier application or patent but published on or after the international filing date

"L" document which may throw doubts on priority claim(s) or which is cited to establish the publication date of another citation or other special reason (as specified)

"O" document referring to an oral disclosure, use, exhibition or other means

"P" document published prior to the international filing date but later than the priority date claimed

"T" later document published after the international filing date or priority date and not in conflict with the application but cited to understand the principle or theory underlying the invention

"X" document of particular relevance; the claimed invention cannot be considered novel or cannot be considered to involve an inventive step when the document is taken alone

"Y" document of particular relevance; the claimed invention cannot be considered to involve an inventive step when the document is combined with one or more other such documents, such combination being obvious to a person skilled in the art

"&" document member of the same patent family

Date of the actual completion of the international search	Date of mailing of the international search report
23 May 2017	23 May 2017
Name and mailing address of the ISA/AU	**Authorised officer**
AUSTRALIAN PATENT OFFICE PO BOX 200, WODEN ACT 2606, AUSTRALIA Email address: pct@ipaustralia.gov.au	Ata Maqbool AUSTRALIAN PATENT OFFICE (ISO 9001 Quality Certified Service) Telephone No. 0262832183

INTERNATIONAL SEARCH REPORT C (Continuation). DOCUMENTS CONSIDERED TO BE RELEVANT		International application No. **PCT/AU2017/050294**
Category*	Citation of document, with indication, where appropriate, of the relevant passages	Relevant to claim No.
X	STAB, D. et al: 'Accelerated mapping of magnetic susceptibility using 3D planes-on-a-paddlewheel (POP) EPI at ultra-high field strength', Special issue research article, 20 October 2016, pages 1-12, wileyonlinelibrary.com, DOI: 10.1002/nbm.3620 Abstract, pages 1-12, figs 1A-1C, 4, 6	1-53
X	US 2016/0069974 A1 (SAMSUNG ELECTRONICS CO., LTD.) 10 March 2016 Figs 1, 2, 5A-5C, 6B, 7; paragraphs 9, 23, 24, 49, 93-108, 119, 123, 129-133, 141-144, 149-150	33-51, 53
X	US 2015/0177353 A1 (THE GENERAL HOSPITAL CORPORATION) 25 June 2015 Figs 1, 3, 4; paragraphs 8-11, 15, 16, 27, 36, 37, 41-45, 58	33-51, 53

INTERNATIONAL SEARCH REPORT Information on patent family members	International application No. **PCT/AU2017/050294**

This Annex lists known patent family members relating to the patent documents cited in the above-mentioned international search report. The Australian Patent Office is in no way liable for these particulars which are merely given for the purpose of information.

Patent Document/s Cited in Search Report		**Patent Family Member/s**	
Publication Number	**Publication Date**	**Publication Number**	**Publication Date**
US 2016/0069974 A1	10 March 2016	US 2016069974 A1	10 Mar 2016
		KR 20160029586 A	15 Mar 2016
		WO 2016036006 A1	10 Mar 2016
US 2015/0177353 A1	25 June 2015	US 2015177353 A1	25 Jun 2015
		US 2013099784 A1	25 Apr 2013
		US 8981776 B2	17 Mar 2015

End of Annex

Due to data integration issues this family listing may not include 10 digit Australian applications filed since May 2001.